Cell

A conserved family of immune effectors cleaves cellular ATP upon viral infection

Graphical abstract

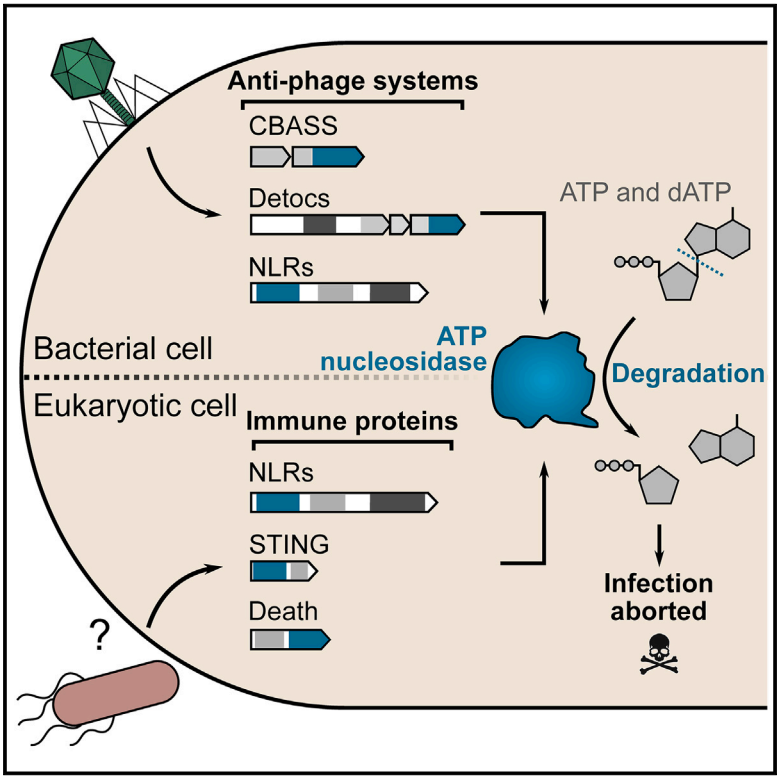

Highlights

- The CBASS immune effector Cap17 is an ATP nucleosidase
- Defensive ATP nucleosidases in bacteria degrade ATP and dATP to block phage
- ATP nucleosidases are part of Detocs, a bacterial two-component anti-phage defense system
- ATP nucleosidases, common in bacteria, are also found in eukaryotic innate immune factors

Authors

Francois Rousset, Erez Yirmiya, Shahar Nesher, ..., Adi Millman, Sarah Melamed, Rotem Sorek

Correspondence

rousset.fra@gmail.com (F.R.), rotem.sorek@weizmann.ac.il (R.S.)

In brief

In diverse organisms across the tree of life, an enzymatic domain blocks viral replication by degrading the essential molecule ATP during infection.

Rousset et al., 2023, Cell *186*, 3619–3631
August 17, 2023
https://doi.org/10.1016/j.cell.2023.07.020

CellPress

Cell

CellPress

Article

A conserved family of immune effectors cleaves cellular ATP upon viral infection

Francois Rousset,[1,*] Erez Yirmiya,[1] Shahar Nesher,[1] Alexander Brandis,[2] Tevie Mehlman,[2] Maxim Itkin,[2] Sergey Malitsky,[2] Adi Millman,[1] Sarah Melamed,[1] and Rotem Sorek[1,3,*]

[1]Department of Molecular Genetics, Weizmann Institute of Science, Rehovot 7610001, Israel

[2]Life Sciences Core Facilities, Weizmann Institute of Science, Rehovot 7610001, Israel

[3]Lead contact

*Correspondence: rousset.fra@gmail.com (F.R.), rotem.sorek@weizmann.ac.il (R.S.)

https://doi.org/10.1016/j.cell.2023.07.020

SUMMARY

During viral infection, cells can deploy immune strategies that deprive viruses of molecules essential for their replication. Here, we report a family of immune effectors in bacteria that, upon phage infection, degrade cellular adenosine triphosphate (ATP) and deoxyadenosine triphosphate (dATP) by cleaving the N-glycosidic bond between the adenine and sugar moieties. These ATP nucleosidase effectors are widely distributed within multiple bacterial defense systems, including cyclic oligonucleotide-based antiviral signaling systems (CBASS), prokaryotic argonautes, and nucleotide-binding leucine-rich repeat (NLR)-like proteins, and we show that ATP and dATP degradation during infection halts phage propagation. By analyzing homologs of the immune ATP nucleosidase domain, we discover and characterize Detocs, a family of bacterial defense systems with a two-component phosphotransfer-signaling architecture. The immune ATP nucleosidase domain is also encoded within diverse eukaryotic proteins with immune-like architectures, and we show biochemically that eukaryotic homologs preserve the ATP nucleosidase activity. Our findings suggest that ATP and dATP degradation is a cell-autonomous innate immune strategy conserved across the tree of life.

INTRODUCTION

The coevolution between viruses and their hosts has driven the emergence and diversification of numerous innate immune strategies in all domains of life. It was recently shown that multiple components of the cell-autonomous innate immune system of animals are also conserved in bacteria, where they function to protect against phage infection.[1] Such conserved immune components include the cGAS-STING pathway,[2–4] nucleotide-binding leucine-rich repeat (NLR) proteins,[5,6] gasdermin-mediated pyroptosis,[7] Toll/interleukin-1 receptor (TIR) domain signaling,[8,9] the RNAi pathway,[10,11] SAMHD1,[12] viperins,[13] and others.[14] Based on these discoveries, it was shown that studying the immune system of bacteria can generate functional knowledge about previously unknown eukaryotic immune mechanisms.[8,14,15]

The cGAS-STING pathway, which senses viral infection in human cells, was shown to be evolutionarily derived from a bacterial defense system called cyclic oligonucleotide-based antiviral signaling system (CBASS).[2–4] Bacterial CBASS immunity relies on a cGAS/DncV-like nucleotidyltransferase (CD-NTase) enzyme that, upon sensing phage infection, produces a cyclic oligonucleotide molecule that binds and activates a cell-killing effector protein.[16] CBASS systems are found in 14% of sequenced bacterial and archaeal genomes and show substantial diversity in their oligonucleotide signals and effector functions.[17,18] CBASS effector proteins can exert their cell-killing function by degrading phage and host DNA,[19–21] disrupting cell membrane integrity,[3,22] or depleting the essential molecule NAD^+.[4,23,24]

A recent analysis of CBASS diversity in prokaryotic genomes revealed that ~10% of type III CBASS systems encode an effector called Cap17, whose molecular function has remained unknown[18] (Figure 1A). In this study, we show that Cap17 is an adenosine triphosphate (ATP) nucleosidase that cleaves ATP and deoxyadenosine triphosphate (dATP) molecules into adenine and (deoxy)ribose-5′-triphosphate during phage infection, depriving the phage of these essential molecules and aborting the infection process. We further show that the Cap17 ATP nucleosidase domain is a distinct immunity domain that is widespread in multiple types of anti-phage systems, including prokaryotic argonauts (pAgo), NLR-like proteins, and others. By studying operons of unknown function that contain the Cap17-like ATP nucleosidase domain, we discovered Detocs, a two-component signal transduction pathway that mediates ATP degradation upon sensing viral infection. Homologs of the Cap17 ATP nucleosidase domain are widespread in eukaryotes, from fungi to animals, where they are associated with various proteins with immune-like architectures. Our study

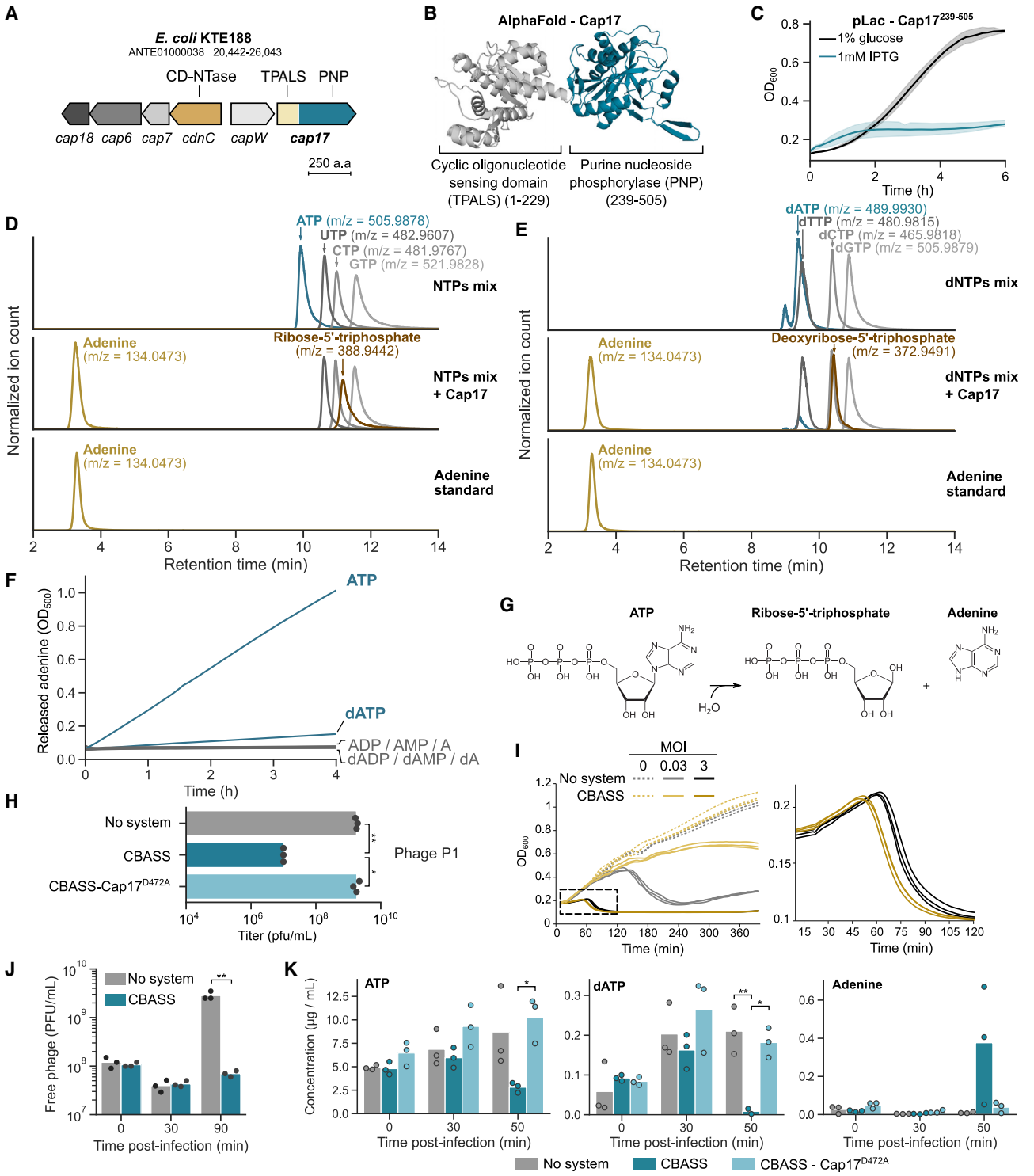

Figure 1. CBASS-associated Cap17 cleaves ATP molecules during phage infection

(A) A type III CBASS from *E. coli* KTE188 encodes the Cap17 effector (Table S1). GenBank accession and genome coordinates are displayed on top. Abbreviations: CD-NTase, cGAS/DncV-like nucleotidyltransferase; TPALS, TIR- and PNP-associating SLOG family; PNP, purine nucleoside phosphorylase.

(B) Predicted AlphaFold2[25,26] structure of Cap17 from *E. coli* KTE188.

(C) Growth curves of *E. coli* K-12 cells expressing the PNP domain from Cap17 (residues 239–505) from the Lac promoter under conditions repressing (1% glucose, black) or inducing expression (1 mM IPTG, blue). Curves show the mean of three replicates with the standard deviation shown as a shaded area.

(legend continued on next page)

defines an immune mechanism that is conserved across the tree of life.

RESULTS

The CBASS effector Cap17 is an ATP nucleosidase

We set out to study the Cap17 protein from the type III CBASS of *E. coli* KTE188, a system that was previously shown to confer resistance against phages[27,28] (Figure 1A). Structural analysis of Cap17 via Alphafold2[25,26] revealed a two-domain architecture with an N-terminal domain predicted to bind the cyclic oligonucleotide messenger (pfam PF18178) and a C-terminal domain of the purine nucleoside phosphorylase (PNP) family PNP_UDP_1 (pfam PF01048, hereafter called PNP) (Figures 1B and S1A). Expression of the PNP domain alone was toxic to *E. coli*, suggesting that it targets an essential host component (Figure 1C). The PNP domain was originally described in diverse housekeeping enzymes involved in nucleotide salvage pathways and is known to cleave the N-glycosidic bond in different nucleosides, separating the nucleobase from the sugar moiety.[29] We therefore suspected that the CBASS Cap17 effector might somehow manipulate cellular nucleotides or nucleosides as part of its anti-phage defensive activity.

We incubated purified Cap17 from *E. coli* KTE188 (Figure S1B) with a mixture of nucleotide triphosphates (NTPs) or deoxynucleotide triphosphates (dNTPs) and subjected the *in vitro* enzymatic reactions to liquid chromatography followed by mass spectrometry (LC-MS). Incubation of purified Cap17 with NTPs revealed a specific consumption of ATP coupled with the formation of two products that we identified as adenine (m/z = 134.047) and ribose-5′-triphosphate (m/z = 388.944) (Figures 1D and S1C). Levels of guanosine triphosphate (GTP), uridine triphosphate (UTP), and cytidine triphosphate (CTP) were not affected by Cap17, suggesting specificity for ATP (Figure 1D). Incubation of Cap17 with dNTPs also revealed consumption of dATP, coupled with the formation of adenine (m/z = 134.047) and deoxyribose-5′-triphosphate (m/z = 372.949) (Figures 1E and S1D). These results suggest that Cap17 specifically cleaves the N-glycosidic bond of (d)ATP to release free adenine, a reaction that was abrogated by a mutation in the catalytic site of the PNP domain (Figures S1E and S1F). Cap17 was unable to release adenine from DNA or RNA, suggesting that it is only active on free nucleotides (Figure S1G). To further assess the substrate specificity of Cap17, we measured its ability to release adenine from various substrates using a xanthine oxidase assay[30] (see STAR Methods). Cap17 activity was markedly higher on ATP than on dATP, and no activity was detected on other adenine-containing nucleotides or nucleosides (Figure 1F). These results demonstrate that Cap17 is an ATP nucleosidase *in vitro* (Figure 1G).

To investigate the immune function of Cap17 during phage infection *in vivo*, we cloned the *E. coli* KTE188 CBASS (Figure 1A; Table S1) with its native promoter into *E. coli* K-12 MG1655 that naturally lacks CBASS and subjected the resulting strain to phage infection. Phage P1 formed ~100-fold fewer plaques on CBASS-expressing cells compared with cells carrying a control vector, confirming the defensive capacity of this CBASS system[27,28] (Figure 1H). A single amino acid mutation in the predicted catalytic site of the Cap17 PNP domain abolished defense, suggesting that the enzymatic activity of Cap17 is essential for CBASS defense (Figure 1H). When grown in liquid medium, CBASS-expressing cultures showed marked survival when infected with P1 phage at low multiplicity of infection (MOI), but the culture collapsed when infected with a high MOI, a hallmark of abortive infection in which infected cells die before the completion of the phage cycle[16,31] (Figure 1I). Concomitantly, infected cells did not produce phage progeny, confirming that this CBASS system prevents phage propagation (Figure 1J).

Analysis of the metabolite content in lysates derived from infected cells showed a marked decrease in ATP levels in CBASS-expressing cells, as well as a complete elimination of dATP 50 min from the onset of infection (Figure 1K). At the same time, an accumulation of adenine was observed (Figure 1K). These changes were not observed in a strain where Cap17 was mutated to disrupt the PNP-active site (D472A) (Figure 1K). Because dATP is substantially less abundant than ATP in *E. coli* cells, the weak activity of Cap17 on dATP compared with ATP (Figure 1F) might still be sufficient to cause the observed

(D) LC-MS analysis of enzymatic reactions with NTPs in the absence (top) or presence (middle) of the Cap17 protein. Peak intensities of each compound were normalized across all samples in the *in vitro* assays. A synthetic adenine standard is shown (bottom). Ribose-5′-triphosphate was identified by MS/MS (Figure S1C).

(E) LC-MS analysis of enzymatic reactions with dNTPs in the absence (top) or presence (middle) of the Cap17 protein. Peak intensities of each compound were normalized across all samples in the *in vitro* assays. A synthetic adenine standard is shown (bottom). Deoxyribose-5′-triphosphate was identified by MS/MS (Figure S1D).

(F) Xanthine oxidase assays measuring adenine release from adenine-containing nucleotides by Cap17, as monitored by absorbance at 500 nm.

(G) A schematic of the Cap17 enzymatic reaction.

(H) Quantification of phage infection efficiency via serial dilution plaque assays. Phage P1 spotted on a lawn of *E. coli* K-12 cells expressing an empty vector (no system), a wild-type CBASS, or a mutated CBASS (CBASS-Cap17^{D472A}). Bars represent the average of three replicates with individual data points overlaid. Stars show significance of a two-sided t test (*$p < 0.05$; **$p < 0.01$).

(I) Growth curves of *E. coli* K-12 cells expressing an empty vector or the CBASS system, infected by phage P1 at an MOI of 0.03 or 3 (or 0 for uninfected cells). The dashed area is magnified on the right. Three replicates are presented as individual curves.

(J) Plaque-forming units of phage P1 sampled from the supernatant of *E. coli* K-12 cells expressing an empty vector or the CBASS system. T = 0 represents initial phage titer prior to infection. Cells were infected at an MOI of 0.1. Bars represent the average of three replicates with individual data points overlaid. Stars show significance of a two-sided t test (**$p < 0.01$).

(K) Quantification of ATP, dATP, and adenine in lysates derived from P1-infected *E. coli* cells expressing an empty vector (no system), a wild-type CBASS, or mutated CBASS (CBASS-Cap17^{D472A}) by LC-MS. Bars represent the average of three replicates with individual data points overlaid. Stars show significance of Tukey multiple comparison tests following analysis of variance (*$0.01 < p \leq 0.05$, **$p \leq 0.01$).

See also Figures S1 and S2.

depletion of dATP. Alternatively, dATP depletion could be a consequence of ATP degradation, given that cellular deoxynucleotides are synthesized from ribonucleotides.[32] A notable drop in the levels of adenosine diphosphate (ADP), deoxyadenosine diphosphate (dADP), and adenosine monophosphate (AMP) was also observed (Figure S2A), but because those nucleotides are poor Cap17 substrates *in vitro* (Figure 1F), we suspect that their levels were affected as a secondary consequence of (d)ATP degradation.

In parallel with the depletion of ATP and dATP from infected CBASS-expressing cells, we observed an accumulation of the three other NTPs (GTP, CTP, and UTP) and dNTPs (deoxyguanosine triphosphate [dGTP], deoxycytidine triphosphate [dCTP], and thymidine triphosphate [TTP]) (Figure S2A). This suggests that Cap17-mediated reduction in ATP and dATP levels decreases the ability of the phage to produce nascent RNA and DNA chains, respectively, resulting in the accumulation of unused non-adenosine (d)NTPs.[12] RNA and DNA sequencing revealed that the presence of CBASS had a modest impact on phage transcription and DNA replication (Figures S2B and S2C), which is likely insufficient to explain why CBASS-expressing cells disintegrate without producing viable phage progeny (Figures 1I and 1J).

It was previously shown that exposure of phage-infected cells to chemicals that deplete cellular energy ("energy poisons" that disrupt the proton motive force) induces premature lysis.[33] This phenomenon, which was observed with multiple different phages, indicates that intracellular energy levels serve to regulate lysis timing by the phage lysis machinery.[33] We therefore hypothesize that ATP depletion by Cap17 causes premature lysis of infected cells (Figure 1I). In agreement with this hypothesis, treatment of P1-infected control cells with the energy poison cyanide 3-chlorophenylhydrazone (CCCP) reduced lysis timing (Figure S2D). Notably, overexpression of the PNP domain of Cap17 in uninfected cells caused a bacteriostatic effect but did not cause cell lysis (Figure 1C), suggesting that the earlier culture collapse of P1-infected CBASS-expressing cells results from the combined effect of Cap17 activity together with phage factors (Figure 1I).

Altogether, our results show that Cap17 is an immune effector whose activation leads to ATP and dATP degradation in response to phage infection, causing pleiotropic effects that prevent phage propagation.

A specialized immune nucleosidase domain functions in multiple defense systems

Given that most proteins that encode PNP domains are housekeeping enzymes involved in nucleotide recycling pathways,[29] the observed antiviral role of the Cap17 PNP domain was puzzling. We therefore wondered whether the PNP domain of Cap17 represents a distinct subfamily that became specialized for an immune function. To examine this possibility, we analyzed a set of ~38,000 bacterial and archaeal genomes and collected ~110,000 proteins in which the PNP_UDP_1 protein domain (pfam PF01048) was detected. We then constructed a phylogenetic tree based on a sequence alignment of the PNP domains only (see STAR Methods). PNP domains clustered into several distinct clades on the tree, with most clades containing PNPs from well-known housekeeping enzymes, including DeoD, XapA, Udp, and MtnN (Figure 2A). The PNP domain of Cap17, however, clustered in a distinct clade that did not include any of the known housekeeping proteins (Figure 2A).

We next examined the gene neighborhood of the 1,038 PNP-containing genes that were found in the Cap17 clade on the phylogenetic tree (Figure 2A). This analysis showed that genes in this clade were very frequently found in the vicinity of known anti-phage systems in microbial genomes (corrected p value $< 10^{-53}$; Figure 2A; Table S3), a metric that was previously shown to be a strong predictor of antiviral activity.[35–38] None of the other major clades on the PNP tree showed a statistically significant enrichment next to known defense systems (Table S3), suggesting that the Cap17 clade represents an evolutionarily derived PNP domain that was adapted for immune functions.

Inspection of the genes from the Cap17 clade showed that this domain is embedded in multiple known anti-phage defense systems (Figure 2B; Table S4). In addition to its presence within CBASS systems, we found this domain in the N terminus of diverse genes of the Avs family.[5,6] These genes represent a large family of immune proteins that are evolutionarily related to human and plant NLRs and inflammasomes.[5,6] In prokaryotes, the C-terminal domain of these proteins senses infection signals, and the N terminus contains an effector domain that leads to cell suicide once infection is sensed.[5] The presence of the PNP domain in the N termini of multiple Avs proteins strongly suggests that it functions as the cell-targeting effector domain in these proteins. We also found the PNP domain in short pAgo systems, which sense phage infection via a pAgo protein and induce cell death via an associated effector protein.[39–42] Effector proteins of short pAgo systems are diverse and include protein domains that disrupt membrane integrity or cleave cellular NAD^+.[39–42] Again, the presence of the PNP domain as an effector of prokaryotic pAgo defense systems indicates that these pAgo systems inflict abortive infection by PNP-mediated ATP degradation (Figure 2B). Finally, we recorded a PNP domain in a defense-associated reverse transcriptase type 8 (DRT8), where it replaces the usual nuclease effector.[43] Altogether, our findings suggest that ATP nucleosidases are immune effectors in diverse antiviral systems in prokaryotes.

A family of two-component systems defends by ATP degradation

Some of the PNP domains from the defensive clade appeared in operons not previously reported as defensive (Table S4). Specifically, we observed multiple cases in which this domain was embedded in an operon whose architecture bears strong similarity to bacterial two-component signal transduction systems[44] (Figures 2B, 3A, and S3A). Such signal transduction systems are ubiquitous in prokaryotes and comprise a sensor kinase that typically senses an environmental signal through its N-terminal domain, triggering autophosphorylation of a conserved histidine residue near the C-terminal kinase domain.[44] The phosphate group is then transferred to a conserved aspartate on the N-terminal receiver domain of the second protein, called the "response regulator." Phosphorylation of the receiver domain activates the C-terminal domain of the response regulator, usually a DNA-binding domain that regulates the expression of target

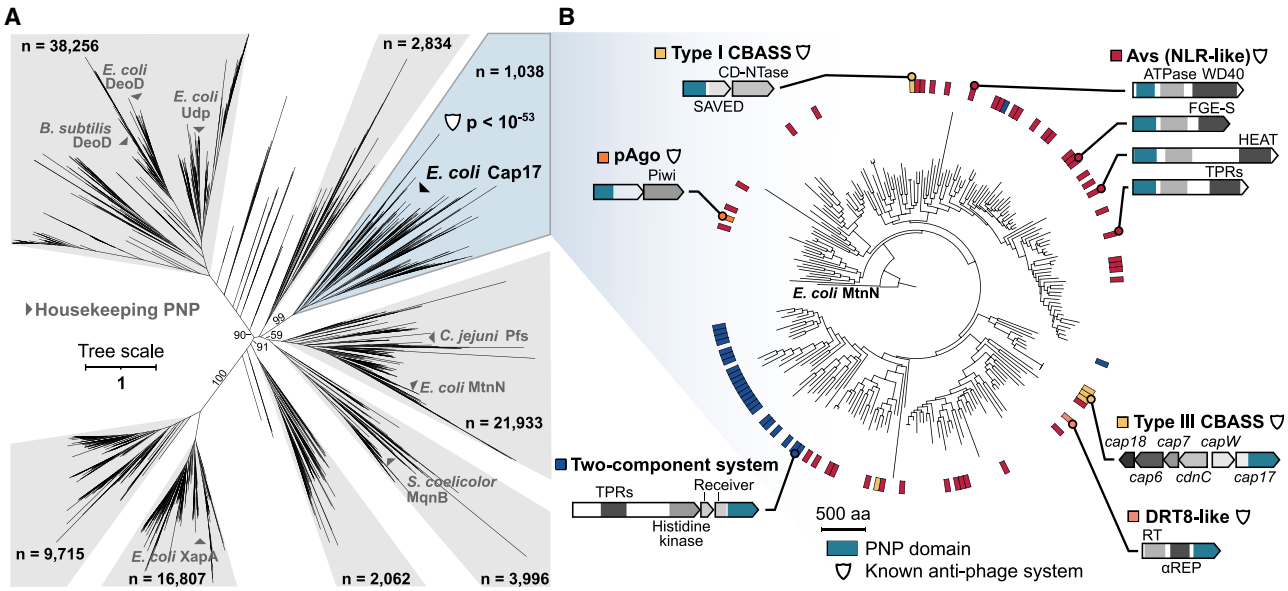

Figure 2. A clade of prokaryotic nucleosidases is associated with anti-phage systems

(A) Phylogenetic tree of prokaryotic PNP domains. Prokaryotic proteins were clustered based on sequence homology, and clusters with homology to the PNP_UDP_1 domain (pfam PF01048) were identified. A representative sequence from each cluster was used to build the tree. The tree is based on the PNP domain only (see STAR Methods). The total number of proteins represented by the representative sequences is shown for each clade. Ultrafast bootstrap values are shown for major branches.[34] Known housekeeping proteins are shown in gray. The p value in the Cap17 clade represents the false discovery rate of a binomial test assessing the association of proteins from this clade with known anti-phage systems (see STAR Methods and Table S3).

(B) A detailed phylogenetic tree of the Cap17 PNP clade (marked blue in A). The PNP domain of *E. coli* MtnN was used as an outgroup. The colored ring represents known or predicted anti-phage systems harboring a PNP domain, with example systems shown as gene cassettes. Abbreviations: pAgo, prokaryotic argonaute; CD-NTase, cGAS/DncV-like nucleotidyltransferase; SAVED, SMODS-associated and fused to various effector domains; NLR, nucleotide-binding leucine-rich repeat; FGE-S, sulfatase-modifying factor enzyme 1; TPR, tetratricopeptide repeat; DRT8, defensive-associated reverse transcriptase type 8.

genes.[44] The PNP-containing operon identified here included a sensor kinase protein and a response regulator protein in which the usual C-terminal DNA-binding domain was replaced by the PNP domain (Figures 3A and S3A). Because PNP domains from the Cap17 clade were associated with multiple defense systems, we hypothesized that this two-component-like operon represents a previously unidentified anti-phage system.

To test this hypothesis, we cloned such an operon from *Vibrio alginolyticus* UCD-32C (Figure 3A; Table S1) under the control of an inducible promoter into *E. coli* K-12 and infected the resulting strain with a diverse panel of phages. The system provided strong resistance against phages T2, T4, T5, T6, and SECphi27, a defense phenotype that required an intact PNP-active site (Figure 3B). Defense was impaired when mutating the conserved histidine on the sensor kinase or when mutating the phosphate-receiving aspartate residue in the response regulator protein (Figures 3B and S3B). These results suggest that the autophosphorylation of the sensor kinase and phosphotransfer to the PNP-containing response regulator are necessary for the defensive activity of this system. We therefore named this system Detocs (defensive two-component system). In addition to the sensor kinase (*dtcA*) and the response regulator (*dtcC*), the Detocs operon also contains a third gene (*dtcB*), whose function is studied below (Figure 3A).

The PNP domain of DtcC from *V. alginolyticus* was highly toxic when expressed alone in *E. coli* (Figure 3C). *In vitro* biochemical assays showed that the purified PNP domain can release adenine from ATP and, to a lesser extent, from dATP but does not affect other NTPs or dNTPs (Figures 3D, 3E, and S3C–S3E). In agreement with this observed biochemical activity, analysis of lysates from T5-infected cells showed a depletion of ATP and dATP in Detocs-expressing cells correlated with an accumulation of adenine, but not when the PNP domain was mutated in the active site (Figures 3F and S3F). These results demonstrate that the PNP domain performs a similar function when found in different defense systems. Detocs triggered growth arrest in cells infected with high MOI of phage T5 (Figure 3G), and infected cells did not release phage progeny (Figure 3H), confirming an abortive infection mechanism. Notably, unlike in CBASS (Figure 1I), growth arrest in response to phage T5 was not associated with cell lysis, suggesting that the energy depletion induced by Detocs does not cause early lysis during T5 infection (Figure 3G). Conversely, infection of Detocs-expressing cells by the phage SECphi27 did lead to cell lysis (Figure S3G), further supporting that premature lysis in response to energy depletion is phage specific.[33]

Although the genetic architecture of Detocs is similar to that of regulatory two-component systems, Detocs also encodes another protein, DtcB, with a standalone receiver domain that is not linked to any effector domain (Figure 3A). We found that a point mutation in the receiving aspartate residue of DtcB rendered Detocs toxic to the cell and that this toxicity was

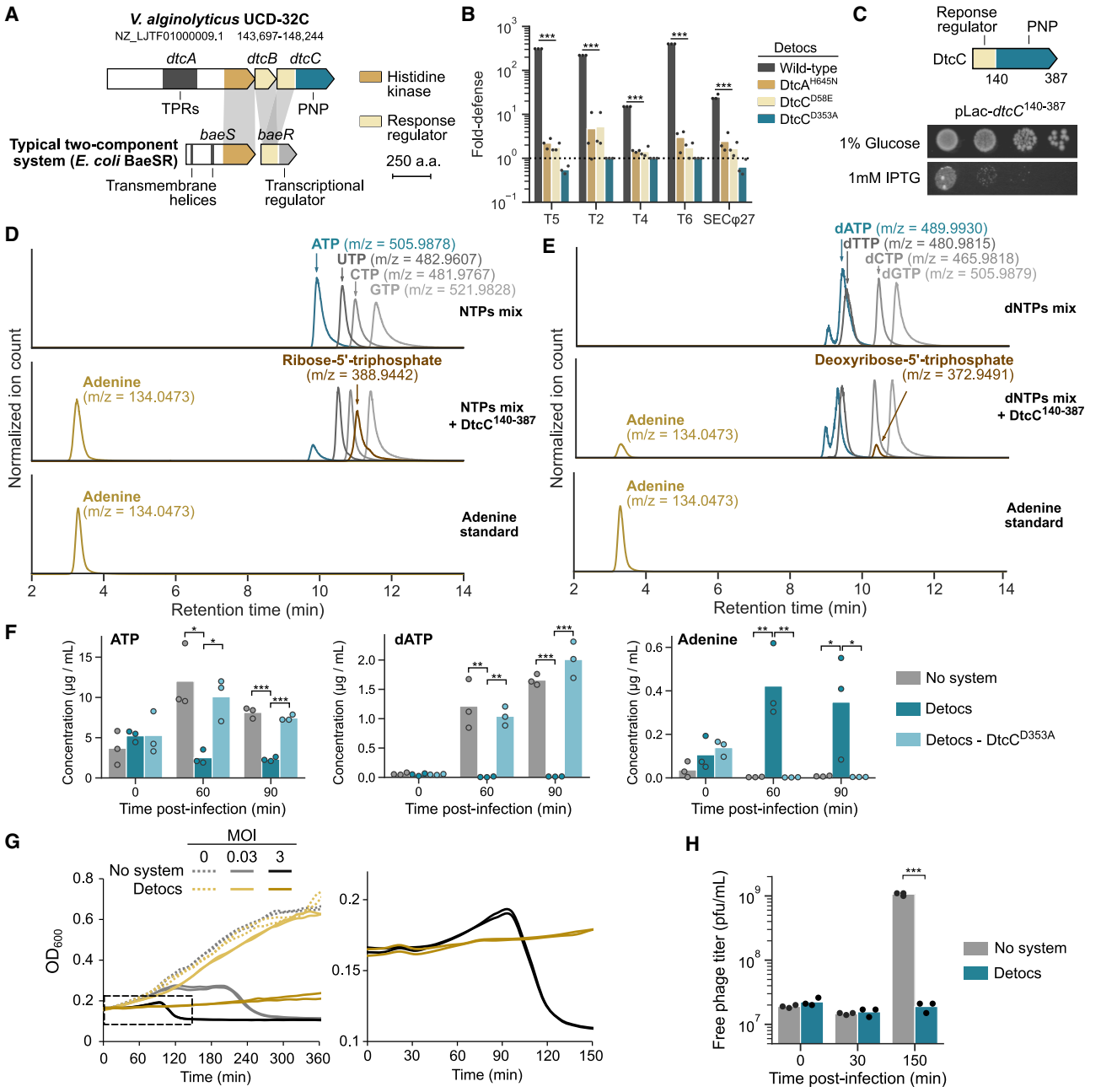

Figure 3. Detocs is a two-component system mediating ATP degradation upon viral infection

(A) A PNP-encoding genetic system from *V. alginolyticus* UCD-32C shares a similar architecture with typical two-component signal transduction systems. The *E. coli* BaeSR two-component system is depicted for comparison of domain architecture. TPR, tetratricopeptide repeat.

(B) Detocs provides phage resistance. Serial dilution plaque assays were performed with phages infecting *E. coli* strains that expressed wild-type *V. alginolyticus* Detocs or Detocs mutated in the phosphate-binding histidine (DtcA^{H645N}), in the phosphate-receiving aspartate (DtcC^{D58E}) or in the predicted catalytic site of the PNP domain (DtcC^{D353A}), all expressed from the pBAD promoter. Fold defense was calculated as the ratio between phage plaque-forming units (PFUs) obtained on control cells and on defense-containing cells. Bars show the mean of three replicates with individual data points overlaid. Stars show significance of Tukey multiple comparison tests following analysis of variance (***p < 0.001). Dotted line indicates the baseline (no defense).

(C) 10-fold serial dilutions of *E. coli* cells expressing the PNP domain from DtcC (residues 140–387) from the Lac promoter were spotted on agar plates under conditions repressing (1% glucose) or inducing expression (1 mM ITPG).

(D) LC-MS analysis of enzymatic reactions with NTPs in the absence (top) or presence (middle) of the PNP domain from DtcC (residues 140–387). A synthetic adenine standard is shown (bottom).

(E) LC-MS analysis of enzymatic reactions with dNTPs in the absence (top) or presence (middle) of the PNP domain from DtcC (residues 140–387). A synthetic adenine standard is shown (bottom).

(legend continued on next page)

dependent on a functional PNP domain (Figure S3H). We therefore propose that DtcB serves as a "buffer" protein that absorbs phosphate signals that result from inadvertent leaky activation of DtcA in the absence of phage infection, thus preventing autoimmunity. In support of this hypothesis, Detocs defense was impaired upon overexpression of DtcB but not upon overexpression of a DtcB variant bearing a point mutation in its receiving aspartate residue (Figure S3I).

Homology-based analyses showed that Detocs systems are found in hundreds of bacterial genomes from diverse phyla[45] (Figures S4A and S4B). Although 80% of Detocs operons encode PNP effectors, in a minority of these operons, the PNP is replaced by other domains known to function as cell-killing effectors in bacterial defense systems, including endonucleases and transmembrane-spanning domains (Table S5). We experimentally tested a Detocs operon with a transmembrane α/β hydrolase effector from *Enterobacter cloacae* JD6301 and found that it was able to efficiently protect *E. coli* against diverse phages (Figure S4C; Table S1).

ATP nucleosidases in eukaryotic innate immune proteins

Our findings demonstrate that the presence of the Cap17-like PNP domain within bacterial proteins of unknown function is predictive of the immune activity of these proteins. This motivated us to ask whether Cap17-like ATP nucleosidases may function in eukaryotes as innate immune proteins because multiple components of the innate immune system of eukaryotes were recently shown to be evolutionarily derived from bacterial defense systems.[1] To this end, we collected from Uniprot ~10,000 eukaryotic proteins encoding the PNP_UDP_1 domain of pfam PF01048. We then reconstructed a phylogenetic tree that includes all detected PNP domains from both eukaryotes and prokaryotes (Figure 4). PNP domains from housekeeping human proteins clustered with PNP domains of housekeeping bacterial proteins, but none of these were included in the defensive clade that contained the PNPs of CBASS and Detocs (Figure 4). However, numerous eukaryotic proteins, whose functions were uncharacterized to date, clustered within the defensive PNP clade, hinting at the presence of an ATP nucleosidase immune activity in eukaryotes (Figure 4; Table S6).

The domain architecture of eukaryotic proteins that cluster within the defensive PNP clade is strongly suggestive of immune functions (Figure 4; Table S6). Specifically, there were hundreds of fungal and coral proteins with an NLR architecture, including a C-terminal-sensing domain, a central nucleotide-binding domain, and an N-terminal PNP domain[47,48] (Figure 4). NLR proteins are abundant pathogen sensors in animals and plants, and fungal NLRs were shown to participate in innate immunity by mediating programmed cell death upon allorecognition,[49] a phenomenon that restricts mycovirus transmission.[50] The presence of the PNP domain in eukaryotic NLRs suggests that these proteins cleave ATP molecules in response to pathogen sensing. Defensive PNP domains were also found in other proteins, combined with additional domains that very strongly indicate an immune function. These included a PNP domain fused to a STING domain in the fungus *Pyrenochaeta*, suggesting that the PNP domain is activated in response to cGAS-like signaling[4,45]; a PNP domain fused to an argonaute protein in *Pochonia chlamydiospora*, suggesting that PNP activity might supplement an RNA interference response[51]; a Gasdermin protein fused to a PNP domain and linked to a nearby caspase-like protease in *Aspergillus niger*, suggesting that this protein might be activated by proteolytic cleavage into a double-edged effector[7,52,53]; and fusions between PNP and death domains, which participate in the assembly of inflammasomes,[54,55] for example, in the sponge *Amphimedon queenslandica* (Figure 4).

Proteins with the Cap17-like PNP domain were also found in arthropods and nematodes, including in the well-studied model organisms *Drosophila melanogaster* (Uniprot accession: Q8MRM6), *Apis mellifera* (Uniprot accession: A0A7M7MVF0), and *Caenorhabditis elegans* (Uniprot accession: H2L0A5) (Figure 4; Table S6). In addition to the PNP domain, these proteins also include a domain that is homologous to the Zα domain found in immune proteins, such as human ZBP1 and ADAR1, where this domain senses foreign nucleic acids with Z-DNA or Z-RNA configuration.[56,57] It is tempting to speculate that these PNP-containing proteins in arthropods and nematodes degrade ATP and dATP upon recognition of foreign nucleic acids.

To test whether the PNP domains of eukaryotic immune-like proteins might mediate (d)ATP degradation, we cloned a death-domain-associated PNP domain from the sponge *A. queenslandica* (Figure 5A). This domain was toxic when expressed in *E. coli* (Figure 5B) and induced a depletion of intracellular ATP (Figure 5C). The purified PNP domain showed preference for ATP over dATP, whereas it was poorly active on other (deoxy)adenylate nucleotides *in vitro* (Figure 5D). By incubating this protein domain with pools of NTPs and dNTPs, we verified that this eukaryotic domain was active only against ATP and dATP (Figures 5E, 5F, S5B, and S5C). We obtained similar results with a PNP domain taken from an NLR-like protein from the fungus *Hyaloscypha variabilis*, which specifically degraded ATP and dATP when tested *in vitro* (Figures S5D–S5F). Taken together, the activity of eukaryotic Cap17-like PNP domains, in addition to their presence within proteins with a typical immune architecture, strongly suggests that ATP degradation is a cell-

(F) Quantification of ATP, dATP, and adenine in lysates derived from T5-infected *E. coli* cells expressing an empty vector (no system), a wild-type Detocs, or mutated Detocs (Detocs-DtcC^{D353A}). Bars represent the average of three replicates with individual data points overlaid. Stars show significance of Tukey multiple comparison tests following analysis of variance (*$0.01 < p \leq 0.05$, **$0.001 < p \leq 0.01$, ***$p < 0.001$).

(G) Growth curves of *E. coli* cells expressing an empty vector or the Detocs system, infected by phage T5 at an MOI of 0.03 or 3 (or 0 for uninfected cells). The dashed area is magnified on the right. Three replicates are presented as individual curves.

(H) Plaque-forming units of phage T5 sampled from the supernatant of *E. coli* cells expressing an empty vector or the Detocs system. T = 0 represents initial phage titer prior to infection. Cells were infected at an MOI of 0.1. Bars represent the average of three replicates with individual data points overlaid. Stars show significance of a two-sided t test (***$p < 0.001$).

See also Figures S3 and S4.

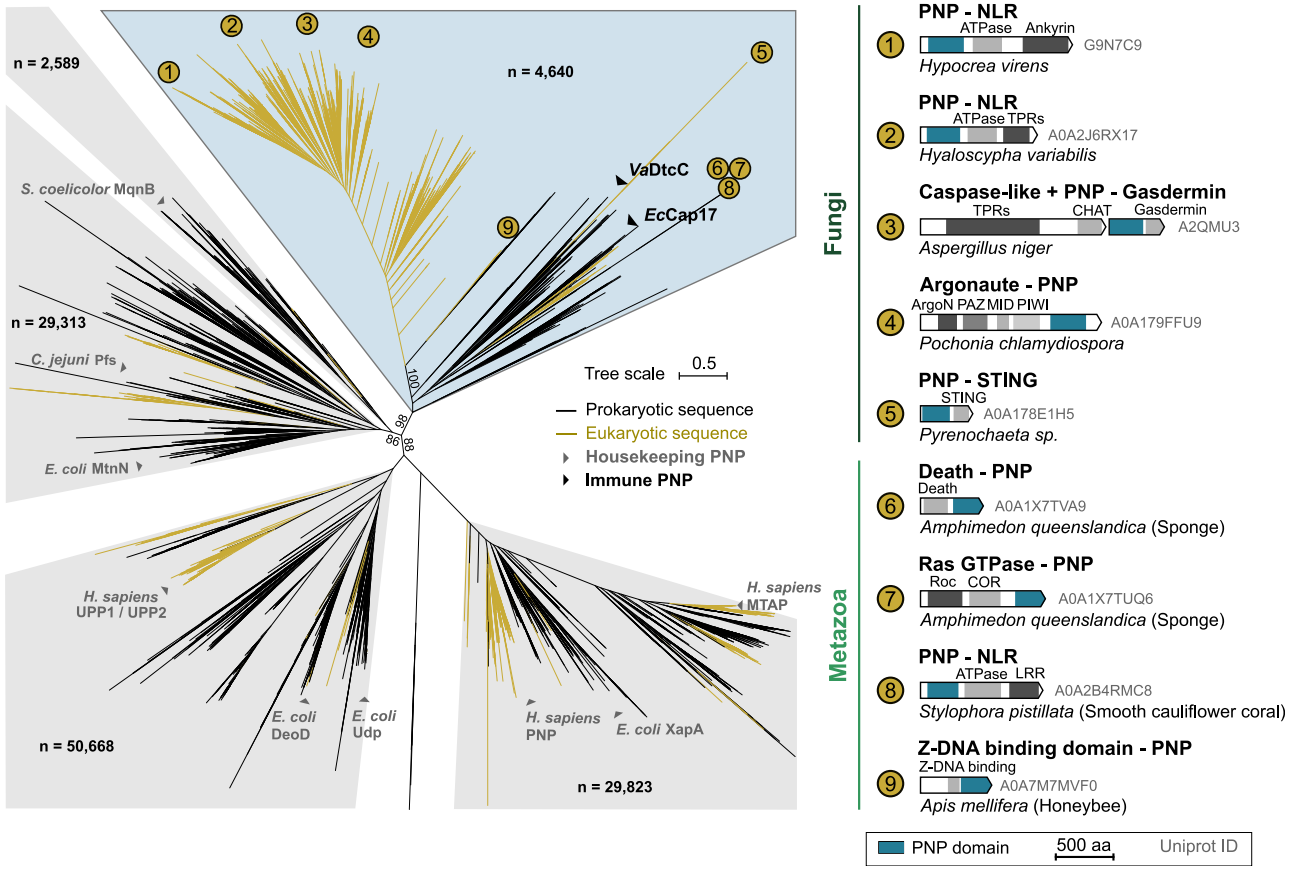

Figure 4. Diverse eukaryotic immune proteins carry Cap17-like PNP effector domains

Phylogenetic tree of prokaryotic and eukaryotic PNP domains. Prokaryotic and eukaryotic proteins were separately clustered based on sequence homology, and a representative sequence from each cluster was used to build the tree. Tree is based on the PNP domain only (see STAR Methods). Ultrafast bootstrap values are shown for major branches.[46] Prokaryotic and eukaryotic PNP domains are shown as black and yellow branches, respectively. PNP domains from known housekeeping proteins are annotated in gray. The immune PNP domains of *V. alginolyticus* DtcC (VaDtcC) and of *E. coli* Cap17 (EcCap17) are annotated in black. The total number of redundant protein sequences represented in each clade is depicted. The architecture of selected eukaryotic homologs is displayed on the right. Abbreviations: NLR, nucleotide-binding leucine-rich repeat; TPR, tetratricopeptide repeat; CHAT, caspase HetF associated with TPRs; PAZ, Piwi Argonaute and Zwille; STING, stimulator of interferon gene; Roc, Ras of complex; COR, C-terminal of Roc; LRR, leucine-rich repeat.

autonomous innate immune strategy in both prokaryotes and eukaryotes.

DISCUSSION

In this study, we describe an immune strategy mediated by a family of enzymatic effectors that degrade ATP and dATP in response to viral infection. This discovery expands the repertoire of immune domains known to target essential metabolites to limit viral replication, including the TIR,[4,23,24,39,58] sirtuin (SIR2),[8,41,42] and SEFIR[38] domains that degrade NAD^+; and dCTP deaminases,[12] dGTPases,[12] and SAMHD1[59] that degrade deoxynucleotides. The central role of ATP makes it an ideal target for degradation in order to simultaneously inhibit multiple cellular processes that are essential for viral propagation. The Cap17 ATP nucleosidase activity separates the adenine base from the sugar moiety, generating free adenine and (deoxy)ribose-5′-triphosphate, a molecule not naturally synthesized by *E. coli* cells to our knowledge. Therefore, it is unlikely that the molecules generated by Cap17 could be efficiently used by cellular pathways to rebuild ATP. Interestingly, ATP and dATP degradation by Cap17 leads to cell lysis during phage P1 infection (Figure 1I), whereas the expression of ATP nucleosidase domains alone leads to growth arrest but does not induce cell lysis (Figure 1C). The phenomenon of early cell lysis following energy depletion was also observed in the context of SIR2, TIR, and SEFIR immunity, in which NAD^+ degradation caused the cells to lyse prematurely after infection by some phages.[8,38,42,58] Our data may suggest that energy depletion during infection not only deprives phages of the energy necessary for their propagation but also serves to dysregulate their lysis machinery,[33] forcing it to prematurely lyse the host cell prior to the completion of the infection cycle.

By analyzing homologs of the Cap17 ATP nucleosidase domain, we discovered Detocs, a family of defensive two-component signal transduction pathways. Two-component signal transduction systems are very abundant in bacteria, where they frequently mediate transcriptional regulation and

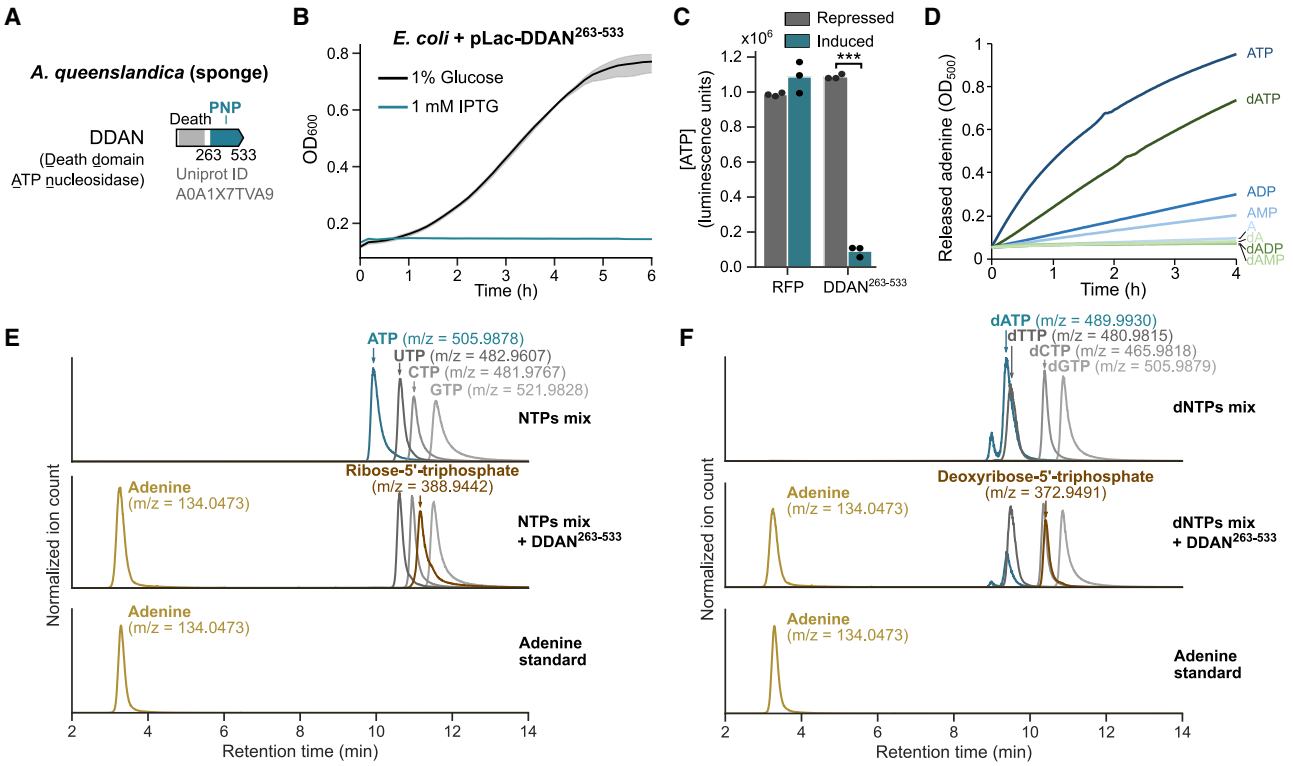

Figure 5. PNP domains associated with eukaryotic immune proteins have ATP nucleosidase activity

(A) The death domain-containing protein (called DDAN here) from the sponge *Amphimedon queenslandica* harbors a C-terminal PNP domain (residues 263–533).

(B) Growth curves of *E. coli* cells expressing the PNP domain from DDAN from the Lac promoter in conditions repressing expression (1% glucose, black) or inducing expression (1 mM ITPG, blue). Curves show the mean of three replicates with the standard deviation shown as a shaded area.

(C) *E. coli* cells carrying a vector expressing red-fluorescent protein (RFP) or the PNP domain from DDAN from the Lac promoter were grown to stationary phase in repressed conditions. Protein expression was then induced by the addition of 1 mM IPTG. Relative intracellular ATP concentration was measured after 2 h of incubation at 37°C using a BacTiter-Glo luminescence assay (Promega). Bars show the mean of three independent replicates with individual data.

(D) Xanthine oxidase assays measuring adenine release from adenine-containing nucleotides by the PNP domain from DDAN, as monitored by absorbance at 500 nm.

(E) LC-MS analysis of enzymatic reactions with NTPs in the absence (top) or presence (middle) of the PNP domain from DDAN. A synthetic adenine standard is shown (bottom).

(F) LC-MS analysis of enzymatic reactions with dNTPs in the absence (top) or presence (middle) of the PNP domain from DDAN. A synthetic adenine standard is shown (bottom).

See also Figure S5.

chemotaxis in response to specific environmental signals.[44] Although some two-component systems were shown to regulate the expression of anti-phage systems,[60,61] our data show that two-component signal transduction pathways were evolutionarily adopted as *bona fide* anti-phage defense systems. The genetic architecture of Detocs supports a mechanism in which phage infection is sensed by the DtcA kinase, which autophosphorylates and transmits the phosphate signal to the DtcC effector to activate it, as previously hypothesized based on a bioinformatic analysis.[45] The system also contains DtcB, an additional protein encoding a single receiver domain, which we hypothesize prevents autoimmunity by scavenging phosphate signals resulting from unintended activation of DtcA. Remarkably, the well-known modularity of two-component systems[44] is preserved in Detocs, in which the ATP nucleosidase effector domain can be replaced by other effector types (Figure S4B), illustrating how swapping effector domains can expand the functional diversity of anti-phage systems.[62] Further biochemical analyses will be necessary to establish the cascade of phosphotransfer within the Detocs system in response to phage infection.

Our evolutionary analyses suggest that immune ATP nucleosidases form an ancient subfamily within the PNP domain family. Based on the topology of the phylogenetic tree, these immune ATP nucleosidases likely emerged in bacteria and were acquired by eukaryotes, possibly on multiple occasions (Figure 4). Our data show that eukaryotic domains of this subfamily preserve ATP and dATP nucleosidase activities *in vitro* and are frequently found in proteins that are very likely to be involved in innate immunity based on their domain architectures. Interestingly, ATP N-glycosidase enzymatic activity has been observed in a sponge lysate,[63,64] but the functional role of this activity remains unknown. Further studies will be necessary to investigate the immune functions of Cap17-like ATP nucleosidases in eukaryotes. Beyond the Cap17-like PNP subfamily, housekeeping PNP

enzymes from nucleotide salvage pathways have been shown to indirectly regulate innate immune functions in humans and in *C. elegans* by affecting nucleoside concentrations,[65,66] illustrating the broad importance of the PNP protein family in the manipulation of cellular nucleotides in immune processes.

In recent years, multiple eukaryotic innate immunity pathways have been shown to have a deep evolutionary origin in prokaryotes.[1,14] Many of the discoveries showing that bacterial defense systems function similarly to their eukaryotic counterparts were enabled by translating prior knowledge of eukaryotic immunity into the prokaryotic world. However, the recent expansion of the known repertoire of anti-phage systems now provides the opportunity to apply the reverse reasoning, i.e., to translate our knowledge of prokaryotic immunity into the eukaryotic world.[8,14,15,38] Our discovery of an immune effector domain that is conserved across the tree of life presents an opportunity to unravel previously unknown functions within the innate immune system of eukaryotes based on bacterial defense against phages.

Limitations of the study

Although we found that purified Cap17 is active *in vitro*, we expect Cap17 activity to be triggered *in vivo* by the signaling molecule that is produced by the associated CD-NTase upon phage infection, as occurs in all known CBASS systems.[16] Further experiments are necessary to confirm this and identify the signal produced by the associated CD-NTase as well as the phage signal that triggers the system. *In vitro* activity of bacterial immune effectors and sensors in the absence of an activation signal is not uncommon and was observed, for example, for the ThsA NAD-degrading effector of the Thoeris defense system,[34] as well as for multiple CD-NTases.[2] *In vitro* activity in the absence of activating signal might stem from overcrowding of the purified protein, simulating the protein oligomerization that is typical of activated effectors of bacterial immune systems.

Although we identified the ATP nucleosidase domain in eukaryotic proteins with typical immune architectures, further studies will be necessary to investigate the immune role of these proteins *in vivo* during pathogen response.

STAR★METHODS

Detailed methods are provided in the online version of this paper and include the following:

- KEY RESOURCES TABLE
- RESOURCE AVAILABILITY
  - Lead contact
  - Materials availability
  - Data and code availability
- EXPERIMENTAL MODEL AND SUBJECT DETAILS
  - Bacterial strains and phages
- METHOD DETAILS
  - Plasmid construction
  - Toxicity assays
  - Protein purification
  - *In vitro* assays and LC-MS polar metabolite analysis
  - Xanthine oxidase assays
  - Plaque assays
  - Liquid infection assays
  - Cell lysate preparation
  - Quantification of nucleotides by LC-MS
  - DNA and RNA sequencing
  - Western Blot
  - Phylogenetic analysis of the PNP domain family
  - Detection of Detocs in prokaryotic genomes

SUPPLEMENTAL INFORMATION

Supplemental information can be found online at https://doi.org/10.1016/j.cell.2023.07.020.

ACKNOWLEDGMENTS

We thank Yao Li, Hunter Toyoda, and Philip Kranzusch for scientific insights; Emily Troemel, Vladimir Lažetić, Jared Nigg, and Carla Saleh for useful discussion on eukaryotic PNP domains; and all members of the Sorek lab for critical comments on the manuscript. F.R. was supported by the Clore Foundation postdoctoral fellowship and by the Dean of Faculty fellowship from the Weizmann Institute of Science. R.S. was supported, in part, by the European Research Council (grant ERC-AdG GA 101018520), the Israel Science Foundation (MAPATS grant 2720/22), the Deutsche Forschungsgemeinschaft (SPP 2330, grant 464312965), the Ernest and Bonnie Beutler Research Program of Excellence in Genomic Medicine, and the Knell Family Center for Microbiology. E.Y. is supported by the Israeli Council for Higher Education (CHE) via the Weizmann Data Science Research Center. A.M. was supported by a fellowship from the Ariane de Rothschild Women Doctoral Program and, in part, by the Israeli Council for Higher Education via the Weizmann Data Science Research Center. M.I. and S. Malitsky are supported by the Vera and John Schwartz Family Center for Metabolic Biology.

AUTHOR CONTRIBUTIONS

F.R., E.Y., and R.S. conceptualized the project. F.R., S.N., and S. Melamed performed genetic analyses and plaque assays. F.R. performed protein purifications and biochemical assays. A.B., T.M., M.I., and S. Malitsky performed LC-MS experiments. F.R. and E.Y. performed evolutionary analyses. F.R. and A.M. detected Detocs in bacterial genomes. F.R. and R.S. wrote the manuscript.

DECLARATION OF INTERESTS

R.S. is a scientific cofounder and advisor of BiomX and Ecophage.

Received: January 16, 2023
Revised: May 18, 2023
Accepted: July 12, 2023
Published: August 17, 2023

REFERENCES

1. Wein, T., and Sorek, R. (2022). Bacterial origins of human cell-autonomous innate immune mechanisms. Nat. Rev. Immunol. *22*, 629–638. https://doi.org/10.1038/s41577-022-00705-4.
2. Whiteley, A.T., Eaglesham, J.B., de Oliveira Mann, C.C., Morehouse, B.R., Lowey, B., Nieminen, E.A., Danilchanka, O., King, D.S., Lee, A.S.Y., Mekalanos, J.J., et al. (2019). Bacterial cGAS-like enzymes synthesize diverse nucleotide signals. Nature *567*, 194–199. https://doi.org/10.1038/s41586-019-0953-5.
3. Cohen, D., Melamed, S., Millman, A., Shulman, G., Oppenheimer-Shaanan, Y., Kacen, A., Doron, S., Amitai, G., and Sorek, R. (2019). Cyclic GMP–AMP signalling protects bacteria against viral infection. Nature *574*, 691–695. https://doi.org/10.1038/s41586-019-1605-5.

4. Morehouse, B.R., Govande, A.A., Millman, A., Keszei, A.F.A., Lowey, B., Ofir, G., Shao, S., Sorek, R., and Kranzusch, P.J. (2020). STING cyclic dinucleotide sensing originated in bacteria. Nature *586*, 429–433. https://doi.org/10.1038/s41586-020-2719-5.

5. Gao, L.A., Wilkinson, M.E., Strecker, J., Makarova, K.S., Macrae, R.K., Koonin, E.V., and Zhang, F. (2022). Prokaryotic innate immunity through pattern recognition of conserved viral proteins. Science *377*, eabm4096. https://doi.org/10.1126/science.abm4096.

6. Kibby, E.M., Conte, A.N., Burroughs, A.M., Nagy, T.A., Vargas, J.A., Whalen, L.A., Aravind, L., and Whiteley, A.T. (2023). Bacterial NLR-related proteins protect against phage. Cell *186*, 2410–2424.e18. https://doi.org/10.1016/j.cell.2023.04.015.

7. Johnson, A.G., Wein, T., Mayer, M.L., Duncan-Lowey, B., Yirmiya, E., Oppenheimer-Shaanan, Y., Amitai, G., Sorek, R., and Kranzusch, P.J. (2022). Bacterial gasdermins reveal an ancient mechanism of cell death. Science *375*, 221–225. https://doi.org/10.1126/science.abj8432.

8. Ofir, G., Herbst, E., Baroz, M., Cohen, D., Millman, A., Doron, S., Tal, N., Malheiro, D.B.A., Malitsky, S., Amitai, G., et al. (2021). Antiviral activity of bacterial TIR domains via immune signalling molecules. Nature *600*, 116–120. https://doi.org/10.1038/s41586-021-04098-7.

9. Essuman, K., Milbrandt, J., Dangl, J.L., and Nishimura, M.T. (2022). Shared TIR enzymatic functions regulate cell death and immunity across the tree of life. Science *377*, eabo0001. https://doi.org/10.1126/science.abo0001.

10. Swarts, D.C., Jore, M.M., Westra, E.R., Zhu, Y., Janssen, J.H., Snijders, A.P., Wang, Y., Patel, D.J., Berenguer, J., Brouns, S.J.J., et al. (2014). DNA-guided DNA interference by a prokaryotic Argonaute. Nature *507*, 258–261. https://doi.org/10.1038/nature12971.

11. Olovnikov, I., Chan, K., Sachidanandam, R., Newman, D.K., and Aravin, A.A. (2013). Bacterial Argonaute samples the transcriptome to identify foreign DNA. Mol. Cell *51*, 594–605. https://doi.org/10.1016/j.molcel.2013.08.014.

12. Tal, N., Millman, A., Stokar-Avihail, A., Fedorenko, T., Leavitt, A., Melamed, S., Yirmiya, E., Avraham, C., Brandis, A., Mehlman, T., et al. (2022). Bacteria deplete deoxynucleotides to defend against bacteriophage infection. Nat. Microbiol. *7*, 1200–1209. https://doi.org/10.1038/s41564-022-01158-0.

13. Bernheim, A., Millman, A., Ofir, G., Meitav, G., Avraham, C., Shomar, H., Rosenberg, M.M., Tal, N., Melamed, S., Amitai, G., et al. (2021). Prokaryotic viperins produce diverse antiviral molecules. Nature *589*, 120–124. https://doi.org/10.1038/s41586-020-2762-2.

14. Cury, J., Mordret, E., Trejo, V.H., Tesson, F., Ofir, G., Poirier, E.Z., and Bernheim, A. (2022). Conservation of antiviral systems across domains of life reveals novel immune mechanisms in humans. https://doi.org/10.1101/2022.12.12.520048.

15. Leavitt, A., Yirmiya, E., Amitai, G., Lu, A., Garb, J., Herbst, E., Morehouse, B.R., Hobbs, S.J., Antine, S.P., Sun, Z.-Y.J., et al. (2022). Viruses inhibit TIR gcADPR signaling to overcome bacterial defense. Nature *611*, 326–331. https://doi.org/10.1038/s41586-022-05375-9.

16. Duncan-Lowey, B., and Kranzusch, P.J. (2022). CBASS phage defense and evolution of antiviral nucleotide signaling. Curr. Opin. Immunol. *74*, 156–163. https://doi.org/10.1016/j.coi.2022.01.002.

17. Tesson, F., Hervé, A., Mordret, E., Touchon, M., d'Humières, C., Cury, J., and Bernheim, A. (2022). Systematic and quantitative view of the antiviral arsenal of prokaryotes. Nat. Commun. *13*, 2561. https://doi.org/10.1038/s41467-022-30269-9.

18. Millman, A., Melamed, S., Amitai, G., and Sorek, R. (2020). Diversity and classification of cyclic-oligonucleotide-based anti-phage signalling systems. Nat. Microbiol. *5*, 1608–1615. https://doi.org/10.1038/s41564-020-0777-y.

19. Lowey, B., Whiteley, A.T., Keszei, A.F.A., Morehouse, B.R., Mathews, I.T., Antine, S.P., Cabrera, V.J., Kashin, D., Niemann, P., Jain, M., et al. (2020). CBASS immunity uses CARF-related effectors to sense 3′–5′- and 2′–5′-linked cyclic oligonucleotide signals and protect bacteria from phage infection. Cell *182*, 38–49.e17. https://doi.org/10.1016/j.cell.2020.05.019.

20. Lau, R.K., Ye, Q., Birkholz, E.A., Berg, K.R., Patel, L., Mathews, I.T., Watrous, J.D., Ego, K., Whiteley, A.T., Lowey, B., et al. (2020). Structure and mechanism of a cyclic trinucleotide-activated bacterial endonuclease mediating bacteriophage immunity. Mol. Cell *77*, 723–733.e6. https://doi.org/10.1016/j.molcel.2019.12.010.

21. Fatma, S., Chakravarti, A., Zeng, X., and Huang, R.H. (2021). Molecular mechanisms of the CdnG-Cap5 antiphage defense system employing 3′,2′-cGAMP as the second messenger. Nat. Commun. *12*, 6381. https://doi.org/10.1038/s41467-021-26738-2.

22. Duncan-Lowey, B., Mcnamara-Bordewick, N.K., Tal, N., Sorek, R., and Kranzusch, P.J. (2021). Effector-mediated membrane disruption controls cell death in CBASS antiphage defense. Mol. Cell *81*, 5039–5051.e5. https://doi.org/10.1016/J.MOLCEL.2021.10.020.

23. Morehouse, B.R., Yip, M.C.J., Keszei, A.F.A., McNamara-Bordewick, N.K., Shao, S., and Kranzusch, P.J. (2022). Cryo-EM structure of an active bacterial TIR–STING filament complex. Nature *608*, 803–807. https://doi.org/10.1038/s41586-022-04999-1.

24. Hogrel, G., Guild, A., Graham, S., Rickman, H., Grüschow, S., Bertrand, Q., Spagnolo, L., and White, M.F. (2022). Cyclic nucleotide-induced helical structure activates a TIR immune effector. Nature *608*, 808–812. https://doi.org/10.1038/s41586-022-05070-9.

25. Mirdita, M., Schütze, K., Moriwaki, Y., Heo, L., Ovchinnikov, S., and Steinegger, M. (2022). ColabFold: making protein folding accessible to all. Nat. Methods *19*, 679–682. https://doi.org/10.1038/s41592-022-01488-1.

26. Jumper, J., Evans, R., Pritzel, A., Green, T., Figurnov, M., Ronneberger, O., Tunyasuvunakool, K., Bates, R., Žídek, A., Potapenko, A., et al. (2021). Highly accurate protein structure prediction with AlphaFold. Nature *596*, 583–589. https://doi.org/10.1038/s41586-021-03819-2.

27. Hobbs, S.J., Wein, T., Lu, A., Morehouse, B.R., Schnabel, J., Leavitt, A., Yirmiya, E., Sorek, R., and Kranzusch, P.J. (2022). Phage anti-CBASS and anti-Pycsar nucleases subvert bacterial immunity. Nature *605*, 522–526. https://doi.org/10.1038/s41586-022-04716-y.

28. Blankenchip, C.L., Nguyen, J.V., Lau, R.K., Ye, Q., Gu, Y., and Corbett, K.D. (2022). Control of bacterial immune signaling by a WYL domain transcription factor. Nucleic Acids Res. *50*, 5239–5250. https://doi.org/10.1093/nar/gkac343.

29. Pugmire, M.J., and Ealick, S.E. (2002). Structural analyses reveal two distinct families of nucleoside phosphorylases. Biochem. J. *361*, 1–25. https://doi.org/10.1042/0264-6021:3610001.

30. Dunn, S.M., Bryant, J.A., and Kerr, M.W. (1994). A simple spectrophotometric assay for plant 5′-deoxy-5′-methylthioadenosine nucleosidase using xanthine oxidase as a coupling enzyme. Phytochem. Anal. *5*, 286–290. https://doi.org/10.1002/PCA.2800050603.

31. Lopatina, A., Tal, N., and Sorek, R. (2020). Abortive infection: bacterial suicide as an antiviral immune strategy. Annu. Rev. Virol. *7*, 371–384. https://doi.org/10.1146/annurev-virology-011620-040628.

32. Greene, B.L., Kang, G., Cui, C., Bennati, M., Nocera, D.G., Drennan, C.L., and Stubbe, J. (2020). Ribonucleotide reductases: structure, chemistry, and metabolism suggest new therapeutic targets. Annu. Rev. Biochem. *89*, 45–75. https://doi.org/10.1146/annurev-biochem-013118-111843.

33. Young, R. (1992). Bacteriophage lysis: mechanism and regulation. Microbiol. Rev. *56*, 430–481. https://doi.org/10.1128/mr.56.3.430-481.1992.

34. Ka, D., Oh, H., Park, E., Kim, J.H., and Bae, E. (2020). Structural and functional evidence of bacterial antiphage protection by Thoeris defense system via NAD^+ degradation. Nat. Commun. *11*, 2816. https://doi.org/10.1038/s41467-020-16703-w.

35. Makarova, K.S., Wolf, Y.I., and Koonin, E.V. (2013). Comparative genomics of defense systems in archaea and bacteria. Nucleic Acids Res. *41*, 4360–4377. https://doi.org/10.1093/nar/gkt157.

36. Doron, S., Melamed, S., Ofir, G., Leavitt, A., Lopatina, A., Keren, M., Amitai, G., and Sorek, R. (2018). Systematic discovery of antiphage defense

systems in the microbial pangenome. Science *359*, eaar4120. https://doi.org/10.1126/science.aar4120.

37. Gao, L., Altae-Tran, H., Böhning, F., Makarova, K.S., Segel, M., Schmid-Burgk, J.L., Koob, J., Wolf, Y.I., Koonin, E.V., and Zhang, F. (2020). Diverse enzymatic activities mediate antiviral immunity in prokaryotes. Science *369*, 1077–1084. https://doi.org/10.1126/science.aba0372.

38. Millman, A., Melamed, S., Leavitt, A., Doron, S., Bernheim, A., Hör, J., Garb, J., Bechon, N., Brandis, A., Lopatina, A., et al. (2022). An expanded arsenal of immune systems that protect bacteria from phages. Cell Host Microbe *30*, 1556–1569.e5. https://doi.org/10.1016/j.chom.2022.09.017.

39. Koopal, B., Potocnik, A., Mutte, S.K., Aparicio-Maldonado, C., Lindhoud, S., Vervoort, J.J.M., Brouns, S.J.J., and Swarts, D.C. (2022). Short prokaryotic Argonaute systems trigger cell death upon detection of invading DNA. Cell *185*, 1471–1486.e19. https://doi.org/10.1016/j.cell.2022.03.012.

40. Zeng, Z., Chen, Y., Pinilla-Redondo, R., Shah, S.A., Zhao, F., Wang, C., Hu, Z., Wu, C., Zhang, C., Whitaker, R.J., et al. (2022). A short prokaryotic Argonaute activates membrane effector to confer antiviral defense. Cell Host Microbe *30*, 930–943.e6. https://doi.org/10.1016/j.chom.2022.04.015.

41. Zaremba, M., Dakineviciene, D., Golovinas, E., Zagorskaitė, E., Stankunas, E., Lopatina, A., Sorek, R., Manakova, E., Ruksenaite, A., Silanskas, A., et al. (2022). Short prokaryotic Argonautes provide defence against incoming mobile genetic elements through NAD^+ depletion. Nat. Microbiol. *7*, 1857–1869. https://doi.org/10.1038/s41564-022-01239-0.

42. Garb, J., Lopatina, A., Bernheim, A., Zaremba, M., Siksnys, V., Melamed, S., Leavitt, A., Millman, A., Amitai, G., and Sorek, R. (2022). Multiple phage resistance systems inhibit infection via SIR2-dependent NAD^+ depletion. Nat. Microbiol. *7*, 1849–1856. https://doi.org/10.1038/s41564-022-01207-8.

43. Mestre, M.R., Gao, L.A., Shah, S.A., López-Beltrán, A., González-Delgado, A., Martínez-Abarca, F., Iranzo, J., Redrejo-Rodríguez, M., Zhang, F., and Toro, N. (2022). UG/Abi: a highly diverse family of prokaryotic reverse transcriptases associated with defense functions. Nucleic Acids Res. *50*, 6084–6101. https://doi.org/10.1093/nar/gkac467.

44. Zschiedrich, C.P., Keidel, V., and Szurmant, H. (2016). Molecular mechanisms of two-component signal transduction. J. Mol. Biol. *428*, 3752–3775. https://doi.org/10.1016/j.jmb.2016.08.003.

45. Burroughs, A.M., and Aravind, L. (2020). Identification of uncharacterized components of prokaryotic immune systems and their diverse eukaryotic reformulations. J. Bacteriol. *202*, 365–385. https://doi.org/10.1128/JB.00365-20.

46. Minh, B.Q., Nguyen, M.A.T., and Von Haeseler, A. (2013). Ultrafast approximation for phylogenetic bootstrap. Mol. Biol. Evol. *30*, 1188–1195. https://doi.org/10.1093/molbev/MST024.

47. Hamada, M., Shoguchi, E., Shinzato, C., Kawashima, T., Miller, D.J., and Satoh, N. (2013). The Complex NOD-Like Receptor Repertoire of the Coral Acropora digitifera Includes Novel Domain Combinations. Mol. Biol. Evol. *30*, 167–176. https://doi.org/10.1093/molbev/MSS213.

48. Dyrka, W., Lamacchia, M., Durrens, P., Kobe, B., Daskalov, A., Paoletti, M., Sherman, D.J., and Saupe, S.J. (2014). Diversity and variability of NOD-like receptors in fungi. Genome Biol. Evol. *6*, 3137–3158. https://doi.org/10.1093/GBE/EVU251.

49. Heller, J., Clavé, C., Gladieux, P., Saupe, S.J., and Glass, N.L. (2018). NLR surveillance of essential SEC-9 SNARE proteins induces programmed cell death upon allorecognition in filamentous fungi. Proc. Natl. Acad. Sci. USA *115*, E2292–E2301. https://doi.org/10.1073/pnas.1719705115.

50. Biella, S., Smith, M.L., Aist, J.R., Cortesi, P., and Milgroom, M.G. (2002). Programmed cell death correlates with virus transmission in a filamentous fungus. Proc. Biol. Sci. *269*, 2269–2276. https://doi.org/10.1098/rspb.2002.2148.

51. Dang, Y., Yang, Q., Xue, Z., and Liu, Y. (2011). RNA interference in fungi: pathways, functions, and applications. Eukaryot. Cell *10*, 1148–1155. https://doi.org/10.1128/EC.05109-11.

52. Clavé, C., Dyrka, W., Turcotte, E.A., Granger-Farbos, A., Ibarlosa, L., Pinson, B., Vance, R.E., Saupe, S.J., and Daskalov, A. (2022). Fungal gasdermin-like proteins are controlled by proteolytic cleavage. Proc. Natl. Acad. Sci. USA *119*, e2109418119. https://doi.org/10.1073/pnas.2109418119.

53. Shi, J., Zhao, Y., Wang, K., Shi, X., Wang, Y., Huang, H., Zhuang, Y., Cai, T., Wang, F., and Shao, F. (2015). Cleavage of GSDMD by inflammatory caspases determines pyroptotic cell death. Nature *526*, 660–665. https://doi.org/10.1038/nature15514.

54. Park, H.H., Lo, Y.C., Lin, S.C., Wang, L., Yang, J.K., and Wu, H. (2007). The death domain superfamily in intracellular signaling of apoptosis and inflammation. Annu. Rev. Immunol. *25*, 561–586. https://doi.org/10.1146/annurev.immunol.25.022106.141656.

55. Yuen, B., Bayes, J.M., and Degnan, S.M. (2014). The characterization of sponge NLRs provides insight into the origin and evolution of this innate immune gene family in animals. Mol. Biol. Evol. *31*, 106–120. https://doi.org/10.1093/molbev/MST174.

56. Brown, B.A., Lowenhaupt, K., Wilbert, C.M., Hanlon, E.B., and Rich, A. (2000). The Zα domain of the editing enzyme dsRNA adenosine deaminase binds left-handed Z-RNA as well as Z-DNA. Proc. Natl. Acad. Sci. USA *97*, 13532–13536. https://doi.org/10.1073/PNAS.240464097.

57. Balachandran, S., and Mocarski, E.S. (2021). Viral Z-RNA triggers ZBP1-dependent cell death. Curr. Opin. Virol. *51*, 134–140. https://doi.org/10.1016/j.coviro.2021.10.004.

58. Tal, N., Morehouse, B.R., Millman, A., Stokar-Avihail, A., Avraham, C., Fedorenko, T., Yirmiya, E., Herbst, E., Brandis, A., Mehlman, T., et al. (2021). Cyclic CMP and cyclic UMP mediate bacterial immunity against phages. Cell *184*, 5728–5739.e16. https://doi.org/10.1016/j.cell.2021.09.031.

59. Goldstone, D.C., Ennis-Adeniran, V., Hedden, J.J., Groom, H.C.T., Rice, G.I., Christodoulou, E., Walker, P.A., Kelly, G., Haire, L.F., Yap, M.W., et al. (2011). HIV-1 restriction factor SAMHD1 is a deoxynucleoside triphosphate triphosphohydrolase. Nature *480*, 379–382. https://doi.org/10.1038/nature10623.

60. Lucas-Elío, P., Molina-Quintero, L.R., Xu, H., and Sánchez-Amat, A. (2021). A histidine kinase and a response regulator provide phage resistance to Marinomonas mediterranea via CRISPR-Cas regulation. Sci. Rep. *111*, 1–13. https://doi.org/10.1038/s41598-021-99740-9.

61. Zhou, C.M., Wu, Q., Wang, B., Lin, P., Wu, M., and Yu, X.J. (2021). Calcium-responsive kinase LadS modulates type I–F CRISPR-Cas adaptive immunity. Biochem. Biophys. Res. Commun. *546*, 155–161. https://doi.org/10.1016/j.bbrc.2021.01.100.

62. Rousset, F., and Sorek, R. (2023). The evolutionary success of regulated cell death in bacterial immunity. Curr. Opin. Microbiol. *74*, 102312. https://doi.org/10.1016/j.mib.2023.102312.

63. Reintamm, T., Lopp, A., Kuusksalu, A., Pehk, T., and Kelve, M. (2003). ATP N-glycosidase – a novel ATP-converting activity from a marine sponge Axinella polypoides. Eur. J. Biochem. *270*, 4122–4132. https://doi.org/10.1046/J.1432-1033.2003.03805.X.

64. Reintamm, T., Vallmann, K., Kolk, K., Päri, M., Lopp, A., Aas-Valleriani, N., and Kelve, M. (2019). Cloning and expression of ATP N-glycosidase from the freshwater sponge Ephydatia muelleri. Biochimie *158*, 126–129. https://doi.org/10.1016/j.biochi.2018.12.018.

65. Tecle, E., Chhan, C.B., Franklin, L., Underwood, R.S., Hanna-Rose, W., and Troemel, E.R. (2021). The purine nucleoside phosphorylase pnp-1 regulates epithelial cell resistance to infection in C. elegans. PLoS Pathog. *17*, e1009350. https://doi.org/10.1371/journal.ppat.1009350.

66. Grunebaum, E., Cohen, A., and Roifman, C.M. (2013). Recent advances in understanding and managing adenosine deaminase and purine nucleoside phosphorylase deficiencies. Curr. Opin. Allergy Clin. Immunol. *13*, 630–638. https://doi.org/10.1097/ACI.0000000000000006.

67. Lee, T.S., Krupa, R.A., Zhang, F., Hajimorad, M., Holtz, W.J., Prasad, N., Lee, S.K., and Keasling, J.D. (2011). BglBrick vectors and datasheets: A synthetic biology platform for gene expression. J. Biol. Eng. *5*, 12. https://doi.org/10.1186/1754-1611-5-12.

68. Chen, I.A., Chu, K., Palaniappan, K., Pillay, M., Ratner, A., Huang, J., Huntemann, M., Varghese, N., White, J.R., Seshadri, R., et al. (2019). IMG/M v.5.0: an integrated data management and comparative analysis system for microbial genomes and microbiomes. Nucleic Acids Res. *47*, D666–D677. https://doi.org/10.1093/nar/gky901.

69. Steinegger, M., and Söding, J. (2017). MMseqs2 enables sensitive protein sequence searching for the analysis of massive data sets. Nat. Biotechnol. *35*, 1026–1028. https://doi.org/10.1038/nbt.3988.

70. Steinegger, M., Meier, M., Mirdita, M., Vöhringer, H., Haunsberger, S.J., and Söding, J. (2019). HH-suite3 for fast remote homology detection and deep protein annotation. BMC Bioinformatics *20*, 473. https://doi.org/10.1186/s12859-019-3019-7.

71. Sievers, F., Wilm, A., Dineen, D., Gibson, T.J., Karplus, K., Li, W., Lopez, R., McWilliam, H., Remmert, M., Söding, J., et al. (2011). Fast, scalable generation of high-quality protein multiple sequence alignments using Clustal Omega. Mol. Syst. Biol. *7*, 539. https://doi.org/10.1038/msb.2011.75.

72. Nguyen, L.-T., Schmidt, H.A., von Haeseler, A., and Minh, B.Q. (2015). IQ-TREE: A fast and effective stochastic algorithm for estimating maximum-likelihood phylogenies. Mol. Biol. Evol. *32*, 268–274. https://doi.org/10.1093/molbev/msu300.

73. Letunic, I., and Bork, P. (2019). Interactive Tree Of Life (iTOL) v4: recent updates and new developments. Nucleic Acids Res. *47*, W256–W259. https://doi.org/10.1093/nar/gkz239.

74. Eddy, S.R. (2011). Accelerated profile HMM Searches. PLoS Comput. Biol. *7*, e1002195. https://doi.org/10.1371/journal.pcbi.1002195.

75. Abby, S.S., Néron, B., Ménager, H., Touchon, M., and Rocha, E.P.C. (2014). MacSyFinder: A program to mine genomes for molecular systems with an application to CRISPR-Cas systems. PLoS One *9*, e110726. https://doi.org/10.1371/journal.pone.0110726.

76. Zheng, L., Cardaci, S., Jerby, L., Mackenzie, E.D., Sciacovelli, M., Johnson, T.I., Gaude, E., King, A., Leach, J.D.G., Edrada-Ebel, R., et al. (2015). Fumarate induces redox-dependent senescence by modifying glutathione metabolism. Nat. Commun. *61*, 1–12. https://doi.org/10.1038/ncomms7001.

77. Pluskal, T., Castillo, S., Villar-Briones, A., and Orešič, M. (2010). MZmine 2: Modular framework for processing, visualizing, and analyzing mass spectrometry-based molecular profile data. BMC Bioinformatics *11*, 1–11. https://doi.org/10.1186/1471-2105-11-395/TABLES/3.

78. Mazzocco, A., Waddell, T.E., Lingohr, E., and Johnson, R.P. (2009). Enumeration of bacteriophages using the small drop plaque assay system. Methods Mol. Biol. *501*, 81–85. https://doi.org/10.1007/978-1-60327-164-6_9.

79. Baym, M., Kryazhimskiy, S., Lieberman, T.D., Chung, H., Desai, M.M., and Kishony, R.K. (2015). Inexpensive multiplexed library preparation for megabase-sized genomes. PLoS One *10*, e0128036. https://doi.org/10.1371/journal.pone.0128036.

80. Dar, D., Shamir, M., Mellin, J.R., Koutero, M., Stern-Ginossar, N., Cossart, P., and Sorek, R. (2016). Term-seq reveals abundant ribo-regulation of antibiotics resistance in bacteria. Science *352*, aad9822. https://doi.org/10.1126/science.aad9822.

81. El-Gebali, S., Mistry, J., Bateman, A., Eddy, S.R., Luciani, A., Potter, S.C., Qureshi, M., Richardson, L.J., Salazar, G.A., Smart, A., et al. (2019). The Pfam protein families database in 2019. Nucleic Acids Res. *47*, D427–D432. https://doi.org/10.1093/nar/gky995.

STAR★METHODS

KEY RESOURCES TABLE

REAGENT or RESOURCE	SOURCE	IDENTIFIER
Antibodies		
primary mouse anti-FLAG antibody	Sigma	Cat#F1804; RRID:AB_262044
HRP-conjugated goat anti-rabbit secondary antibody	Thermo Scientific	Cat#31460: RRID:AB_228341
Bacterial and virus strains		
E. coli K-12 MG1655	American Type Culture Collection (ATCC)	ATCC 47076;Genbank: NC_000913
NEB 5-alpha Competent *E. coli*	New England BioLabs	Cat#C2987H
SECphi27	Doron et al.[36]	Genbank: LT961732.1
T5	Udi Qimron	Genbank: AY543070.1
T4	Udi Qimron	Genbank: AF158101.6
T6	German Collection of Microorganisms and Cell Cultures GmbH (DSMZ)	DSM 4622; Genbank: MH550421.1
T2	German Collection of Microorganisms and Cell Cultures GmbH (DSMZ)	DSM 16352; Genbank: LC348380.1
P1	Udi Qimron	Genbank: NC_005856.1
Chemicals, peptides, and recombinant proteins		
Isopropyl β-d-1-thiogalactopyranoside (IPTG)	Inalco	Cat#1758-1400
L-Arabinose	GoldBio	Cat#A300
ATP	Merck	Cat#A1852-1VL
ADP	Merck	Cat#D6000
AMP	Sigma	Cat#01930
Adenosine	Sigma	Cat#A9251
dATP	Thermo Scientific	Cat#R0141
dADP	Alfa Aesar	Cat#J65307
dAMP	Sigma	Cat#D6375
Deoxyadenosine	Sigma	Cat#D7400
Adenine	Sigma	Cat#A2786
NTPs (ATP, GTP, CTP, UTP) (MAXIscript SP6/T7 Transcription Kit)	Ambion	Cat#AM1322
dNTPs (dATP, dGTP, dCTP, dTTP)	New England BioLabs	Cat#N0447L
Xanthine Oxidase	Roche	Cat#10110434001
iodonitrotetrazolium chloride	Sigma	Cat#I8377
20X Bolt MES SDS Running Buffer	ThermoFisher	Cat#B0002
20X Bolt transfer buffer	Thermo Scientific	Cat#BT00061
Critical commercial assays		
KLD enzyme mix	New England Biolabs	Cat#M0554S
NEBuilder® HiFi DNA Assembly Master Mix	New England Biolabs	Cat#E2621L
NEBExpress Ni-NTA Magnetic Beads	New England Biolabs	Cat#S1423L
BacTiter-Glo Microbial Cell Viability Assay	Promega	Cat#G8230
Oligonucleotides		
Primers, see Table S7	This paper	N/A
Recombinant DNA		
pSG1	Doron et al.[36]	N/A
pBAD-GFP	Bernheim et al.[13]	N/A

(*Continued on next page*)

Continued

REAGENT or RESOURCE	SOURCE	IDENTIFIER
pBbA6c-RFP	Lee et al.[67]	Addgene Cat#35290
pET28-SUMO	Leavitt et al.[15]	N/A
Software and algorithms		
Integrated Microbial Genomes (IMG)	Chen et al.[68]	https://img.jgi.doe.gov/m/
MMseqs2	Steinegger and Söding[69]	https://github.com/soedinglab/mmseqs2
HH-suite3	Steinegger et al.[70]	https://github.com/soedinglab/hh-suite
Clustal-omega version 1.2.4	Sievers et al.[71]	http://www.clustal.org/omega/clustalo-api/
IQtree version 1.6.5	Nguyen et al.[72]	http://www.iqtree.org/
iTOL	Letunic and Bork[73]	https://itol.embl.de/
DefenseFinder v1.2	Tesson et al.[17]	https://github.com/mdmparis/defense-finder
Hmmer version 3.3.2	Eddy et al.[74]	http://hmmer.org/
MacSyFinder v1	Abby et al.[75]	https://github.com/gem-pasteur/macsyfinder

RESOURCE AVAILABILITY

Lead contact

Further information and requests for resources and reagents should be directed to the lead contact, Rotem Sorek (rotem.sorek@weizmann.ac.il).

Materials availability

This study did not generate new unique reagents.

Data and code availability

All presented data is available in the supplementary tables. This paper does not report original code.

EXPERIMENTAL MODEL AND SUBJECT DETAILS

Bacterial strains and phages

E. coli NEB 5-alpha (New England Biolabs) was used as a cloning strain. *E. coli* K-12 MG1655 was used for phage-related experiments while *E. coli* BL21(DE3) was used for protein purifications. *Bacillus subtilis* BEST7003 was kindly provided M. Itaya. Unless mentioned otherwise, cells were grown in MMB (LB + 0.1 mM $MnCl_2$ + 5 mM $MgCl_2$, with or without 1.5% agar) with the appropriate antibiotics: ampicillin (100 μg/mL), chloramphenicol (30 μg/mL) or kanamycin (50 μg/mL). Phages used in this study are detailed in Table S2 and in the Key resources table.

METHOD DETAILS

Plasmid construction

The type III CBASS system from *E. coli* KTE188 (Genbank: ANTE01000038)[27] was synthesized by Genscript together with its native promoter and terminator sequences and cloned into plasmid pSG1,[36] yielding pSG1-CBASS (Table S1). Detocs systems from *V. alginolyticus* UCD-32C (Genbank: NZ_LJTF01000009.1) and from *Enterobacter cloacae* JD6301 (Genbank: JDWH01000005.1) were synthesized by Twist Bioscience as gene fragments and assembled into the pBAD plasmid[13] under the arabinose-inducible pBAD promoter by Gibson assembly (New England Biolabs) (Table S1). Point mutations were introduced using the KLD Enzyme mix (New England Biolabs) (Table S7) and were verified by whole-plasmid sequencing (Plasmidsaurus). PNP domains from *Hyaloscypha variabilis* and *Amphimedon queenslandica* were synthesized by Twist Bioscience as gene fragments. All PNP domains tested for toxicity were cloned into the pBbA6c vector[67] (Addgene plasmid # 35290) under the IPTG-inducible Lac promoter.

Toxicity assays

To measure the toxicity of PNP domains, overnight cultures of *E. coli* K-12 MG1655 cells expressing the PNP domain from *E. coli* Cap17, *V. alginolyticus* DtcC, *H. variabilis* NLRN or *A. queenslandica* DDAN on the pBbA6c vector were diluted 100-fold in MMB + chloramphenicol supplemented with 1% glucose or 1 mM IPTG. Growth was followed by OD_{600} measurement every 10 min on a Tecan Infinite200 plate reader.

Protein purification

DNA sequences encoding the proteins to purify were cloned onto the pET28-SUMO vector[15] by Gibson assembly (Table S8). Plasmids were transformed into *E. coli* BL21(DE3) and clones were selected on LB medium supplemented with kanamycin. Overnight cultures of each resulting strain were grown in LB supplemented with kanamycin to OD_{600} of ~0.8-1 and protein expression was induced by the addition of 0.5 mM IPTG (Inalco). Cultures were further incubated for 20 h at 16°C in the case of Cap17 or for 3 h at 37°C in the case of the PNP domains from *V. alginolyticus*, *H. variabilis* and *A. queenslandica*. Cells were harvested by centrifugation (5,000 g – 12 min) and resuspended in wash buffer (20 mM sodium phosphate buffer pH 7.4, 300 mM NaCl, 20 mM imidazole, 0.05% Tween20 supplemented with cOmplete Protease Inhibitor Cocktail tablet (Roche)). Resuspended cells were then transferred to a FastPrep Lysing Matrix B 2 ml tube (MP Biomedicals) and lysed using a FastPrep bead beater for 40 s at 6 $m.s^{-1}$. After centrifugation (12,000 g – 10 min), the supernatant was bound to NEBExpress Ni-NTA Magnetic Beads (NEB) for 1 h at 4°C with rotation. Beads were washed 3 times with wash buffer and once with Ulp1 buffer (40 mM Tris-HCl pH 7.5, 250 mM NaCl, 250 mM sucrose, 2 mM $MgCl_2$). The His-SUMO tag was cleaved on beads using Ulp1 protease produced in-house in Ulp1 buffer for 2 h at 25°C. Cleaved products were collected from the suspension and analyzed by SDS-PAGE and Coomassie staining. Proteins were flash-frozen and stored at -80°C until use.

In vitro assays and LC-MS polar metabolite analysis

The substrate specificity of purified enzymes was assessed by incubating each of them with either a mix of NTPs (Ambion AM1322) or a mix of dNTPs (New England Biolabs N0447L) (final concentration: 100 μM each). Cap17 was also incubated with 50 ng/μL of lambda DNA (NEB #N3011S) or control RNA (Ambion MicrobExpress) to measure a possible release of adenine from nucleic acids. All reactions were performed in triplicates in a volume of 100 μL, in 100 mM sodium phosphate buffer (pH 7.4) with 500 nM enzymes for 1 h at 37°C, except for reactions with the PNP domain from *H. variabilis* which were performed with 1 μM enzyme for 4 h at 37°C. Before the injection into the LC-MS, samples were centrifuged twice (13,000 rpm) to remove possible precipitants, and transferred to a high-performance liquid chromatography (HPLC) vial. Samples were analyzed as described previously[76] with minor modifications described below. Briefly, analysis was performed using Acquity I class UPLC System combined with mass spectrometer Q Exactive Plus Orbitrap™ (Thermo Fisher Scientific), which was operated in a negative ionization mode. The MS spectra were acquired with 70.000 resolution, scan range of 100 – 800 m/z. For the identification of the compounds, we used a data-dependent acquisition, top 5 method. The LC separation was done using the SeQuant Zic-pHilic (150 mm × 2.1 mm) with the SeQuant guard column (20 mm × 2.1 mm) (Merck). The mobile phase B was acetonitrile and the mobile phase A was 20 mM ammonium carbonate with 0.1% ammonia hydroxide in a 80:20 solution (v/v) of double-distilled water and acetonitrile. The flow rate was kept at 200 $\mu l.min^{-1}$, and the gradient was as follows: 75% of B (0-2min), decreased to 25% of B (2-14 min), 25% of B (14-18min), increased to 75% of B (18-19 min), 75% of B (19-23 min). Adenine was identified using a synthetic standard run (Sigma A2786). Data were analyzed using MZmine 2.53.[77] For each compound, peak intensities were normalized across all samples.

Xanthine oxidase assays

The substrate specificity of PNP enzymes on adenylate nucleotides was refined using a xanthine oxidase assay.[30] Briefly, the oxidation of released adenine to 2,8-dihydroadenine by xanthine oxidase is coupled to the reduction of two iodonitrotetrazolium chloride (INT) molecules into formazan which absorbs at 500 nm. Reactions were performed in 100 μL with 1 mM INT (Sigma I8377), 0.035 units of xanthine oxidase (Roche 10110434001) and 200 μM of each substrate (ATP, ADP, AMP, adenosine, dATP, dADP, dAMP and deoxyadenosine) in 100 mM sodium phosphate buffer (pH 7.4). Reactions were started by the addition of purified PNP enzymes to a final concentration of 200 nM, except for the PNP domain from *H. variabilis* which was added to a final concentration of 1 μM. Absorbance at 500 nm was followed on a Tecan Infinite200 plate reader.

Plaque assays

All phages used in this study are listed in Table S2. Phages were amplified from single plaques in liquid cultures of *E. coli* K-12 MG1655 at 37°C in MMB medium until culture collapse. Cultures were centrifuged (4,000 g x 10 min) and the supernatants were passed through 0.2 μm filters.

Plaque assays were performed as previously described.[78] *E. coli* K-12 MG1655 carrying anti-phage systems (pSG1-CBASS or pBAD-Detocs) or control plasmids (pSG1 or pBAD) were grown overnight at 37°C in MMB medium supplemented with ampicillin. Then, 300 μL of each culture was mixed with 30 mL of molten MMB + 0.5% agar supplemented with 0.2% arabinose in the case of pBAD and pBAD-Detocs strains. The mixture was poured on 12 x 12 cm plates and left to dry for 1 h. Tenfold dilutions of phages were prepared in MMB and 10 μL of each dilution was dropped onto the plates. Plates were incubated overnight at 37°C (pSG1 and pSG1-CBASS) or 25°C (pBAD and pBAD-Detocs). Plaque-forming units (PFUs) were counted the next day.

Liquid infection assays

Overnight cultures of *E. coli* K-12 MG1655 carrying anti-phage systems (pSG1-CBASS or pBAD-Detocs) or control plasmids (pSG1 or pBAD) were diluted 100-fold in MMB-ampicillin with (pBAD and pBAD-Detocs) or without (pSG1 and pSG1-CBASS) 0.2% arabinose and grown to an optical density at 600nm (OD_{600}) of 0.3. Then, 190 μL of cultures were transferred to a 96-well plate and

infected with phage P1 at 37°C (pSG1 and pSG1-CBASS) or with T5 at 25°C (pBAD and pBAD-Detocs) at various MOIs. Growth was followed by OD_{600} measurement every 5 min on a Tecan Infinite200 plate reader.

Propagation of phage P1 and T5 on control and defense-expressing cells was measured by infecting exponential cultures at OD_{600} ~0.3 with P1 or T5 at MOI of ~0.1. The infected cultures were sampled at the indicated time points, spun down (14,000 g – 1 min) and the free phage titer was assessed in the supernatant by plaque assays on *E. coli* K-12 MG1655 as described above.

Cell lysate preparation

For CBASS, overnight cultures of *E. coli* K-12 MG1655 carrying pSG1, pSG1-CBASS or pSG1-CBASS-Cap17^{D472A} were diluted 100-fold in 200 mL of MMB + ampicillin and grown to OD_{600} ~0.3 at 37°C with shaking (200 rpm). Then, 50 mL of cultures were sampled (Time 0) and the remaining cultures were infected with ~10^{11} pfus of phage P1 (MOI ~3). After 30 min and 50 min, 50 mL of the culture were sampled. For Detocs, sampling was performed similarly with phage T5 and the following exceptions: (i) MMB + ampicillin was supplemented with 0.2% arabinose, (ii) cultures were incubated at 25°C with shaking (200 rpm), (iii) cultures were sampled 60 min and 90 min post-infection. Following sampling, each sample was centrifuged (4,000 g – 7 min) at 4°C and cell pellets were flash-frozen in a bath of ethanol in dry ice. All pellets were thawed on ice, resuspended in 600 μL of cold 100 mM sodium phosphate buffer (pH 7.4), transferred to FastPrep Lysing Matrix B 2-ml tubes (MP Biomedicals, catalog no. 116911100) and lysed using a FastPrep bead beater for 40 s at 6 $m.s^{-1}$. Samples were centrifuged (12,000 g – 10 min) and supernatants were passed through 3 kDa Amicon Ultra-0.5 Centrifugal Filter Units (Merck Millipore, catalogue no. UFC500396) for 45 min at 12,000 g at 4°C. Filtrates were used for LC-MS analysis for nucleotide quantification.

Quantification of nucleotides by LC-MS

Quantification of metabolites was carried out using an Acquity I-class UPLC system coupled to Xevo TQ-S triple quadrupole mass spectrometer (Waters, US). The UPLC was performed using an Atlantis Premier BEH Z-HILIC column (2.1 x 100 mm, 1.7 um; Waters). Mobile phase A was 80% of 20mM ammonium carbonate, pH 9.25 in acetonitrile and mobile phase B was acetonitrile. The flow rate was kept at 300 $\mu l.min^{-1}$ consisting of a 0.8 min hold at 80% B, followed by a linear gradient decrease to 25% B during 4.6 min. The column temperature was set at 35°C, and the injection volume was 3 μl. An electrospray ionization interface was used as an ionization source. Analysis was performed in positive ionization mode. Metabolites (d)GTP, (d)ATP, TTP/UTP, (d)CTP, (d)ADP, (d)AMP, (d)A, and adenine were detected using multiple-reaction monitoring, using argon as the collision gas. Quantification was made using a standard curve in 0.001–5 $\mu g.mL^{-1}$ concentration range. $^{13}C_{10}$-ATP (Sigma 710695) and $^{15}N_5$-AMP (Sigma 662658) were added to standards and samples as internal standards to get 1 and 0.5 μM, respectively. TargetLynx (Waters) was used for data analysis.

DNA and RNA sequencing

Overnight cultures of *E. coli* K-12 MG1655 carrying pSG1 or pSG1-CBASS were diluted 100-fold in 4 mL of MMB + ampicillin and grown at 37°C. When OD_{600} reached ~0.3, cells were infected with phage P1 at an MOI of ~3 and further incubated at 37°C. Before infection (time 0), and 30 min and 50 min after infection, 1 mL of culture was collected and added to 10 μL of pre-chilled overnight culture of *Bacillus subtilis* BEST7003 used as a spiked-in control. Samples were centrifuged at 4°C (16,000 g – 30 s) and pellets were flash-frozen in a bath of ethanol in dry ice. The remaining volume was infected with phage P1 at an MOI of ~3 and further incubated at 37°C. Sample collection was repeated 30 min and 50 min after infection. For DNA sequencing, total DNA was extracted from pellets using the QIAGEN DNeasy blood and tissue kit (cat. #69504). Libraries were prepared for Illumina sequencing using a modified Nextera protocol as previously described.[79] For RNA sequencing, pellets were resuspended in 100 μl of 2 $mg.ml^{-1}$ lysozyme in 10 mM Tris-HCl and 1 mM EDTA pH 8.0 and incubated at room temperature for 3 min. One milliliter of TRI-reagent (MRC) was added and samples were vortexed for 10 s before the addition of 200 μl chloroform. Following another vortexing step, the samples were left at room temperature for 5 min and centrifuged (16,000 g – 10min) at 4 °C. The upper phase was added to 500 μl of ice-cold isopropanol and samples were incubated at -20 °C for 1 h for RNA precipitation. Samples were then centrifuged (16,000–30min) at 4 °C and the RNA pellet was washed twice with ice-cold 70% ethanol, air-dried and resuspended in 30 μl water. RNA levels were measured using Nanodrop. All RNA samples were treated with TURBO DNase following the manufacturer's instructions (Life technologies, AM2238). Ribosomal RNA depletion and RNA-seq libraries were prepared as previously described,[80] except that all reaction volumes were reduced by a factor of 4. All libraries were sequenced on an Illumina NextSeq500 sequencer. Reads were aligned to the genomes of *E. coli* K-12 MG1655 (Genbank NC_000913), *B. subtilis* BEST7003 (Genbank AP012496.1) and phage P1 (Genbank NC_005856.1) as described previously.[80] Read counts for each sample were normalized to the number of reads mapping the *B. subtilis* BEST7003 genome.

Western Blot

Overnight cultures of *E. coli* cells expressing the 3xFLAG-tagged Detocs variants were diluted 100-fold in MMB supplemented with ampicillin and 0.2 % arabinose. When OD reached OD~0.4, 350 μL of cultures were harvested, pellets were resuspended in 100 μL of 1x Bolt LDS Sample Buffer (Thermo Scientific cat #B0007) supplemented with 50 mM DTT. Samples were incubated at 95°C for 3 min and 10 μL were separated by 4-12% Bis-Tris SDS-PAGE (Thermo Scientific cat# NW04122BOX) in 1X MES SDS Running Buffer (ThermoFisher catalogue no. B0002) for 25 min at 200 V. Proteins were transferred to a nitrocellulose membrane (Invitrogen cat # LC2001) for 1h at 10V in 1x transfer buffer (Thermo Scientific cat# BT00061), blocked with 5% milk in TBS-T, and probed with a

primary mouse anti-FLAG antibody (Sigma F1804, diluted 1:5,000 in 3% BSA in TBS-T) overnight at 4°C. Visualization of the primary antibody was performed using HRP-conjugated goat anti-rabbit secondary antibody (Thermo Scientific cat #31460; 1:10,000 dilution in TBS-T) and incubation with ECL solution (Merck Millipore cat# WBLUF0500).

Phylogenetic analysis of the PNP domain family

Protein sequences of all genes in 38,167 bacterial and archaeal genomes were downloaded from the Integrated Microbial Genomes (IMG) database[68] in October 2017. Proteins with a hit to pfam PF01048 were collected and bacterial and archaeal sequences were separated. Proteins from each group were filtered for redundancy using the 'clusthash' option of MMseqs2 (release 12-113e3)[69] using the '–min-seq-id 0.9' parameter and then clustered using the 'cluster' option with the '–single-step-clustering' flag. For each cluster, the representative sequence defined by MMseqs2 was collected and searched against the Pfam database[81] using hhsearch[70] with default parameters. Cluster representatives with a hit to pfam PF01048 with an e-value equal to or lower than 0.01 and spanning at least 100 residues were selected and the sequence of the PNP domain was extracted. All PNP domains from selected cluster representatives were aligned using Clustal-omega version 1.2.4[71] with default parameters. The resulting multiple-sequence alignment was used to compute a tree using IQtree version 1.6.5[72] using parameters -m LG -nt 1 -nm 5000. Node support was computed using 1000 iterations of the ultrafast bootstrap function in IQtree (option -bb 1000).[46] All trees were visualized with iTOL.[73]

To find clades of PNP-containing genes that are significantly associated with defense systems (Figure 2A), we collected all non-redundant PNP-containing genes and ran DefenseFinder v1.2[17] on their genomes of origin. Then, for each clade, we calculated the fraction of PNP-encoding genes found in the genomic neighborhood of known anti-phage systems (where the genomic neighborhood was defined as 10 genes on each side of the PNP-encoding gene). On the other hand, the fraction of defense-associated genes expected by chance was computed for each clade by dividing the total number of genes located in the neighborhood of anti-phage systems by the total number of genes in the genomes of origin. These values were used to assess whether proteins from each clade colocalize with anti-phage systems more frequently than expected by chance, using a binomial test and FDR correction of the p-value (Table S3).

PNP domain sequences from the Cap17 clade were collected and a new tree was computed as described above, using the PNP domain of *E. coli* MtnN (IMG gene ID 2519179855) as an outgroup (Figure 2B). Members of this clade were manually inspected for known genetic architectures of anti-phage systems.

To investigate the presence of ATP nucleosidases in eukaryotes, 10,176 eukaryotic proteins harboring a PNP domain (pfam PF01048) were collected from the Pfam database web page.[81] These proteins were grouped in 2,571 clusters based on sequence homology and searched for protein domains as described above. Similarly, cluster representatives with a hit to pfam PF01048 with an e-value equal to or lower than 0.01 and spanning at least 100 residues were selected and the sequence of the PNP domain was extracted. Prokaryotic and eukaryotic PNP sequences were aligned and a tree was computed as described above. Node support was computed using 5000 iterations of the ultrafast bootstrap function in IQtree (option -bb 5000).[46] Arthropod and nematode proteins from the Cap17 clade with a Zα domain were expanded to the model species *D. melanogaster* (CG12065) and *C. elegans* (H14E04.2) by blastp search against the Uniprot database.

Detection of Detocs in prokaryotic genomes

Homologs of DtcA, DtcB and DtcC were collected from the above-described protein clusters. For each protein, homologs were aligned using Clustal-omega[71] and the resulting multi-sequence alignment was used to build an HMM profile using the hmmbuild function of hmmer (version 3.3.2).[74] MacSyFinder[75] was then used to search Detocs using the three HMM profiles, requiring all three genes to be present with up to one foreign gene between each Detocs gene. The resulting detected systems were manually inspected for false positives and classified by effector type.

Supplemental figures

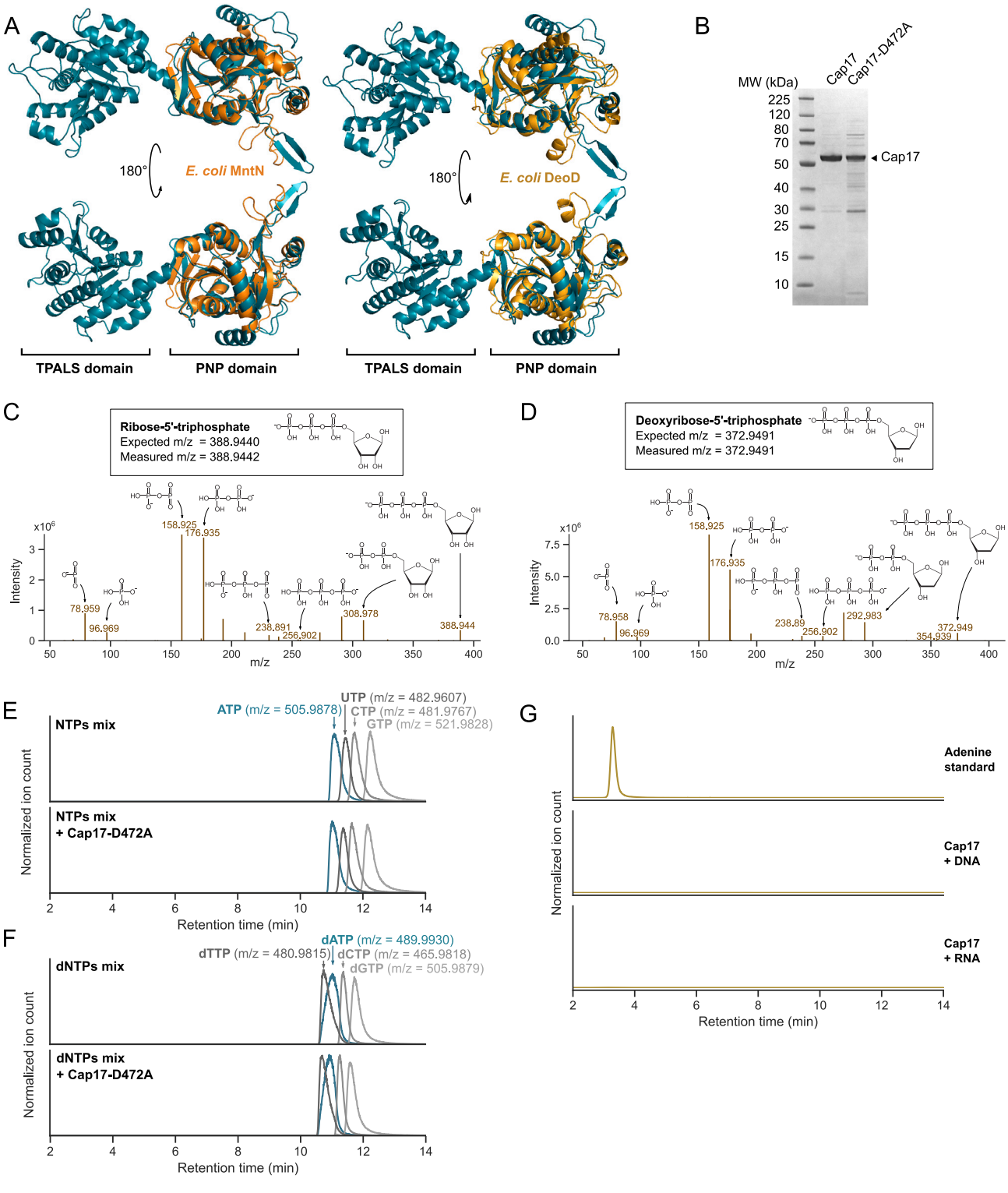

(legend on next page)

Figure S1. Properties of Cap17, related to Figure 1

(A) Structural homology of the Cap17 PNP domain with housekeeping PNP enzymes. The structure of *E. coli* Cap17 was predicted using AlphaFold2[25,26] and aligned to the experimentally determined structures of MtnN (PDB: 1NC1) and DeoD (PDB: 1ECP). Abbreviations: TPALS, TIR- and PNP-associating SLOG family; PNP, purine nucleoside phosphorylase.

(B) SDS-PAGE analysis and Coomassie staining of protein pull-downs of wild-type and mutated Cap17. The expected molecular mass is 54.3 kDa.

(C) MS/MS fragmentation spectra of the product of ATP degradation. The peak of m/z = 388.9442 identified as a conversion product of ATP by Cap17 (Figure 1D) was subjected to MS/MS, supporting the identification of this product as ribose-5′-triphosphate.

(D) MS/MS fragmentation spectra of the product of dATP degradation. The peak of m/z = 372.9491 identified as a conversion product of dATP by Cap17 (Figure 1E) was subjected to MS/MS, supporting the identification of this product as deoxyribose-5′-triphosphate.

(E) Mutated Cap17 does not convert ATP. LC-MS analysis of enzymatic reactions with NTPs in the presence of a catalytic PNP mutant of Cap17. Peak intensities of each compound were normalized across all samples in the *in vitro* assays. Representative of three replicates.

(F) Mutated Cap17 does not convert dATP. LC-MS analysis of enzymatic reactions with dNTPs in the presence of a catalytic PNP mutant of Cap17. Peak intensities of each compound were normalized across all samples in the *in vitro* assays. Representative of three replicates.

(G) Cap17 is inactive on DNA and RNA. Cap17 was incubated with DNA or RNA *in vitro*, and reactions were analyzed by LC-MS. Mass chromatograms of ions with the mass of adenine (m/z = 134.0473) are shown, together with an adenine standard. Representative of three replicates.

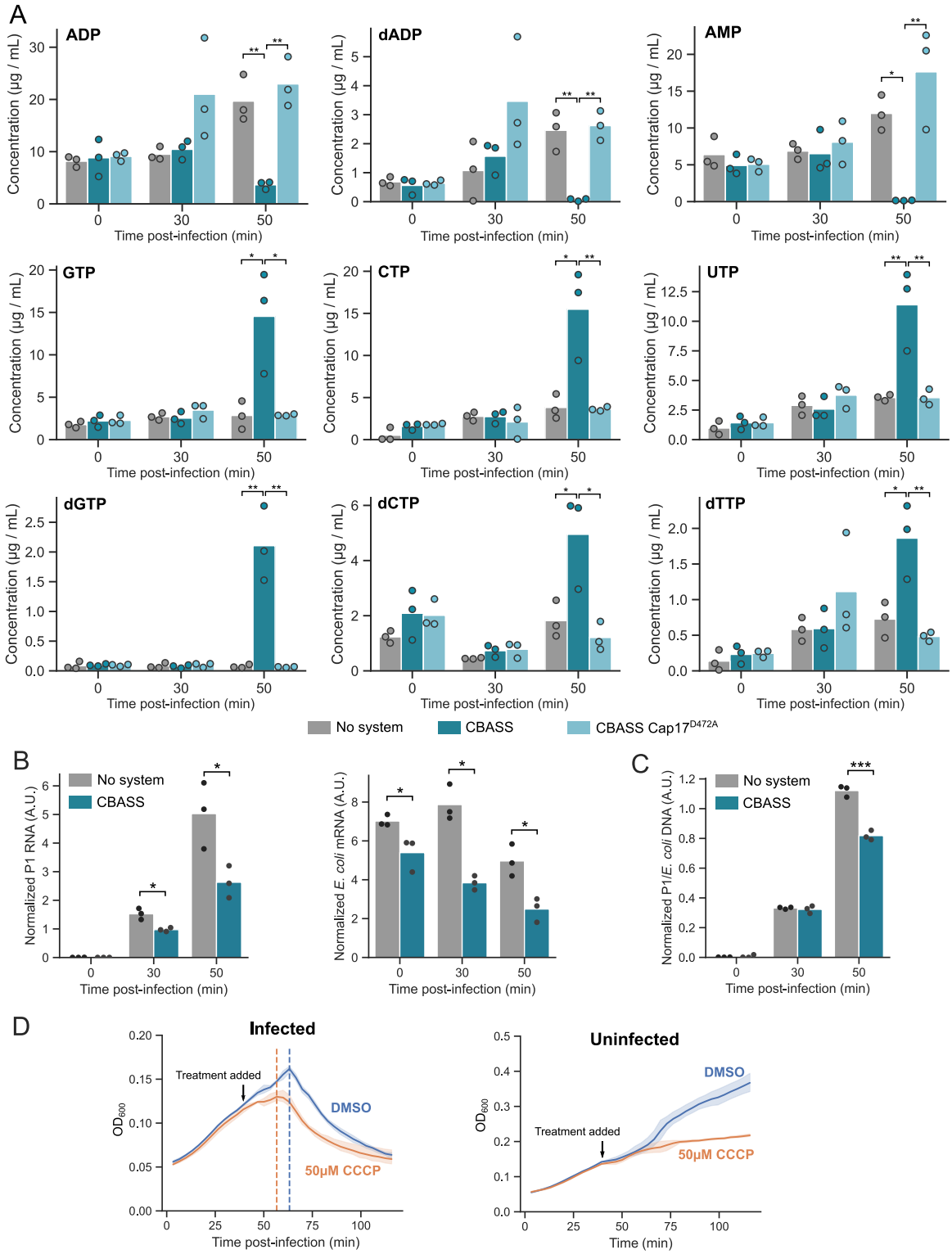

Figure S2. Intracellular effects of Cap17 activity during infection by phage P1, related to Figure 1

(A) Nucleotide concentrations during P1 infection. *E. coli* cells carrying an empty vector (no system) or a vector expressing a wild-type (CBASS) or a mutated CBASS (CBASS-Cap17^{D472A}) were infected by phage P1, and nucleotide concentrations in cell lysates were measured by HPLC. Bars show the mean of three independent replicates with individual data points overlaid. Stars show significance of Tukey multiple comparison tests following analysis of variance (*$0.01 < p \leq 0.05$, **$0.001 < p \leq 0.01$, ***$p < 0.001$).

(legend continued on next page)

(B) RNA from P1-infected *E. coli* cells expressing a control vector or the CBASS system was sequenced. The number of phage P1 (left) or *E. coli* (right) mRNA reads normalized to a spike-in control is shown.
(C) DNA from P1-infected *E. coli* cells expressing a control vector or the CBASS system was sequenced. The ratio of phage to *E. coli* reads after normalization to a spike-in control is shown.
(B and C) Bars show the mean of three independent replicates with individual data points overlaid. Stars show significance levels of a two-sided t test (*$p < 0.05$; ***$p < 0.001$).
(D) Effects of energy depletion during infection. *E. coli* cells were infected with phage P1 at a multiplicity of three (left) or left uninfected (right), and DMSO or 50 μM cyanide 3-chlorophenylhydrazone (CCCP) were added after 40 min. Growth was followed by optical density at 600 nm. Curves show the mean of three replicates with the standard deviation shown as a shaded area.

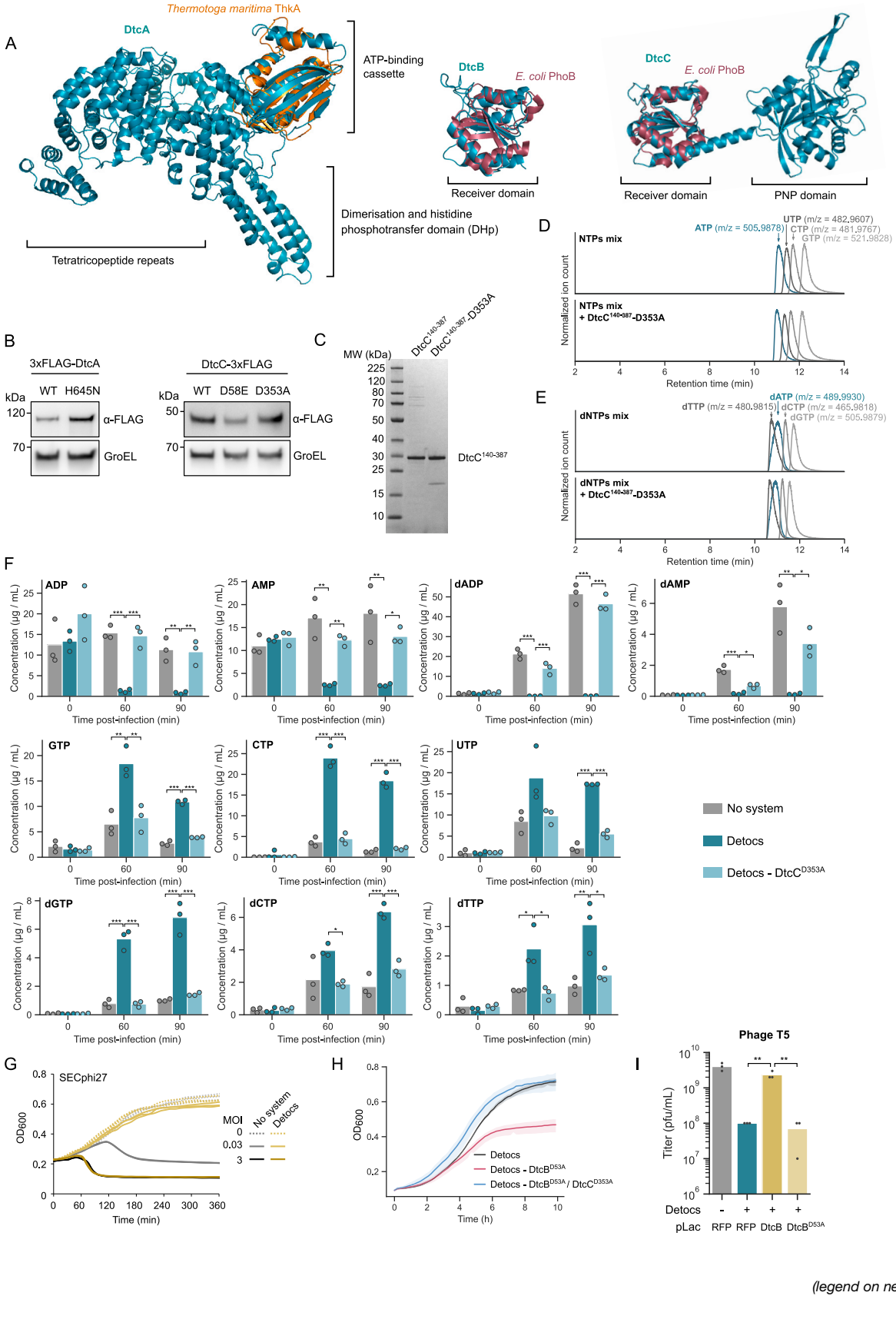

(legend on next page)

Figure S3. *In vitro* and *in vivo* activity of Detocs, related to Figure 3

(A) Detocs is homologous to two-component systems. The AlphaFold2[25,26] structural prediction of DtcA was aligned to the experimentally determined crystal structure of the histidine kinase domain of ThkA from *Thermotoga maritima* (PDB: 3AOZ). The AlphaFold2 structural predictions of DtcB and DtcC were aligned to the experimental structure of the receiver domain of PhoB from *E. coli* (PDB: 1ZES).

(B) Western blot analysis of 3xFLAG-tagged DtcA and DtcC and their catalytic mutants shown in Figure 3B.

(C) SDS-PAGE analysis and Coomassie staining of protein pull-downs of the wild-type ($DtcC^{140–387}$) and mutated ($DtcC^{140–387}$-D353A) PNP domains of DtcC. The expected molecular mass is 27.5 kDa.

(D) Mutated PNP does not convert ATP. LC-MS analysis of enzymatic reactions with NTPs in the presence of a catalytic PNP mutant of $DtcC^{140–387}$. Peak intensities of each compound were normalized across all samples in the *in vitro* assays. Representative of three replicates.

(E) Mutated PNP does not convert dATP. LC-MS analysis of enzymatic reactions with dNTPs in the presence of a catalytic PNP mutant of $DtcC^{140–387}$. Peak intensities of each compound were normalized across all samples in the *in vitro* assays. Representative of three replicates.

(F) Nucleotide concentrations during T5 infection. *E. coli* cells carrying an empty vector (no system) or a vector expressing a wild-type (Detocs) or a mutated Detocs (Detocs-$DtcC^{D353A}$) were infected by phage T5, and nucleotide concentrations in cell lysates were measured by HPLC. Bars show the mean of three independent replicates with individual data points overlaid. Stars show significance of Tukey multiple comparison tests following analysis of variance (*$0.01 < p \leq 0.05$, **$0.001 < p \leq 0.01$, ***$p < 0.001$).

(G) Growth curves of *E. coli* cells expressing an empty vector or the Detocs system, infected by phage SECphi27 at an MOI of 0.03 or 3 (or 0 for uninfected cells). Three replicates are shown as individual curves.

(H) A point mutation in the receiver domain of DtcB is toxic in a PNP-dependent manner. Growth curves of *E. coli* cells expressing a wild-type Detocs (black), a Detocs with a point mutation in the phosphate-receiving aspartate of DtcB (red), or a Detocs with such a mutation combined with a point mutation in the PNP catalytic site of DtcC (blue), as measured by optical density at 600 nm. Curves show the mean of three replicates with the standard deviation shown as a shaded area.

(I) Overexpression of DtcB cancels Detocs-mediated defense. Quantification of phage infection efficiency via serial dilution plaque assays of phage T5 on *E. coli* cells carrying a control or Detocs-expressing vector, combined with the overexpression of either a control protein (RFP), wild-type DtcB, or DtcB mutated in the phosphate-receiving aspartate ($DtcB^{D53A}$), all expressed from the pBbA6c vector with 0.5 mM IPTG. Bars represent the average of three replicates with individual data points overlaid. Stars show significance of Tukey multiple comparison tests following analysis of variance (**$p < 0.01$).

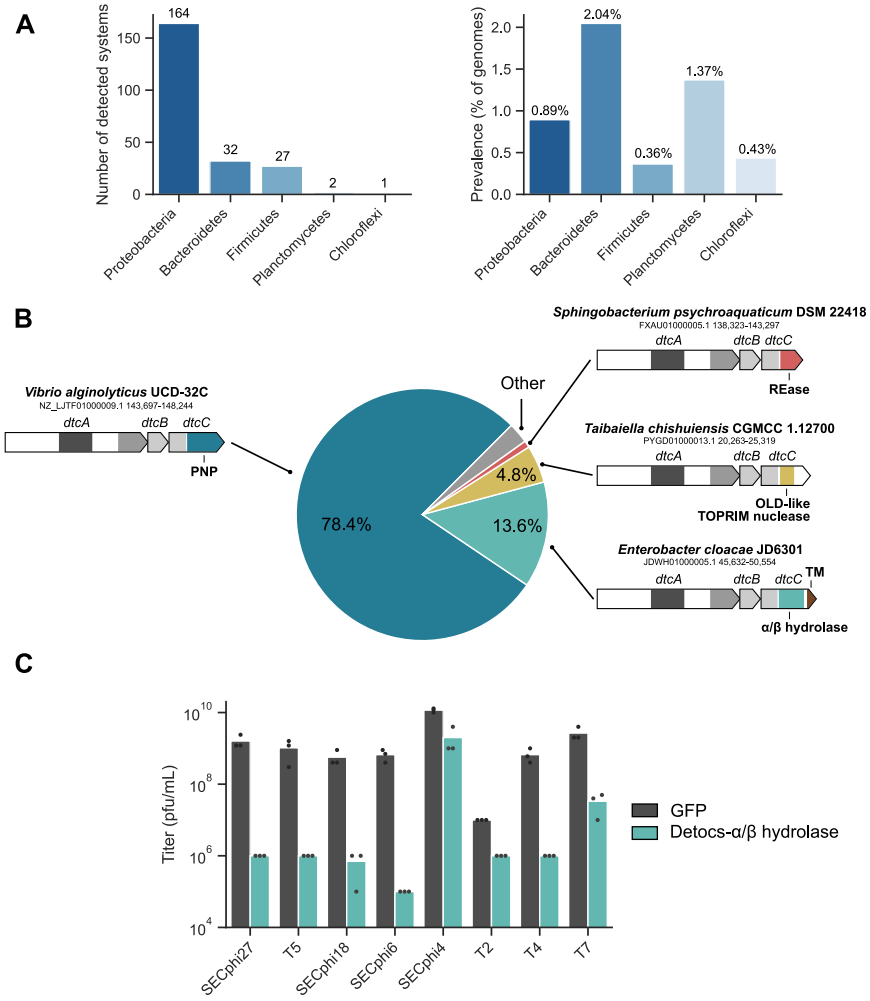

Figure S4. Detocs in the bacterial pangenome, related to Figure 3

(A) Detection of Detocs in bacterial genomes. For phyla where Detocs is found, the number of systems (left) and the percentage of genomes carrying Detocs (right) are shown.

(B) Distribution of types of effector domains in Detocs. Examples of systems are shown, with accession numbers and genome coordinates provided. Abbreviations: REase, restriction endonuclease (pfam PF18742); TOPRIM, topoisomerase-primase (pfam PF20469); TM, transmembrane.

(C) A Detocs system from *Enterobacter cloacae* JD6301 with a transmembrane α/β hydrolase effector provides broad phage resistance in *E. coli*.

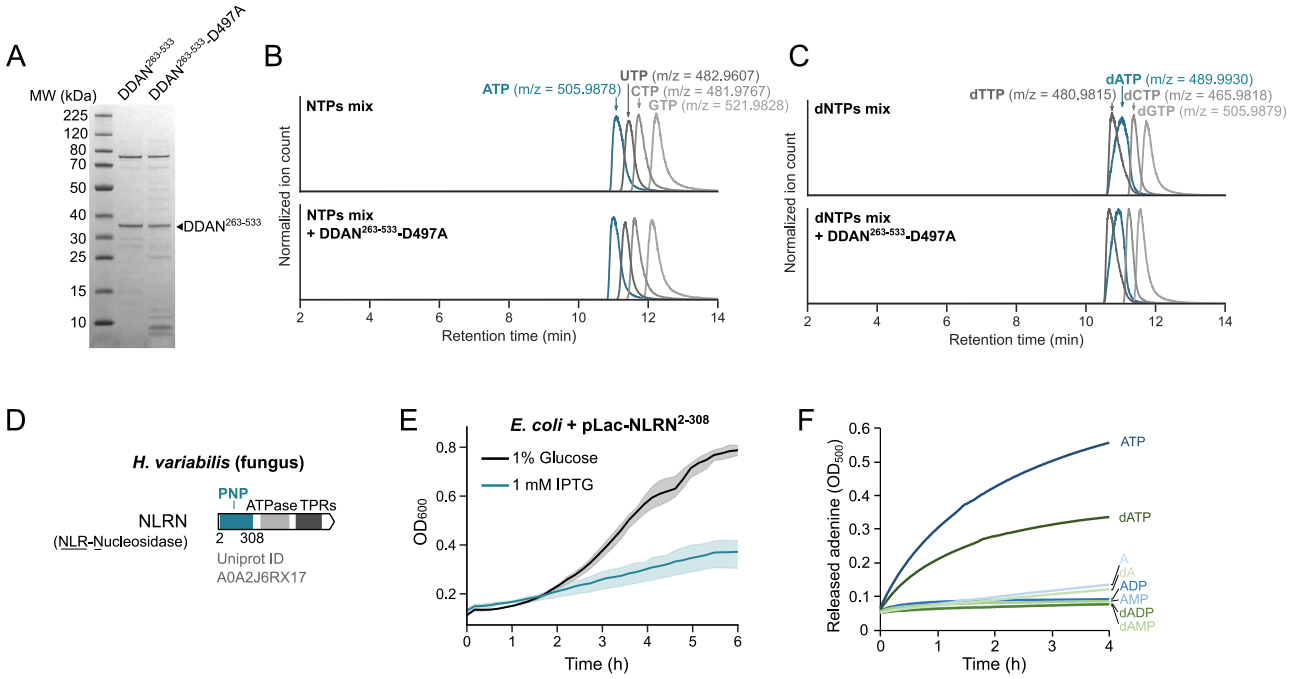

Figure S5. Enzymatic activity of eukaryotic Cap17-like PNP domains, related to Figure 5

(A) SDS-PAGE analysis and Coomassie staining of protein pull-downs of the wild-type (DDAN$^{263–533}$) and mutated (DDAN$^{263–533}$-D497A) PNP domains of DDAN. The expected molecular mass is 29.8 kDa.

(B) Catalytic mutant of DDAN does not convert ATP. LC-MS analysis of enzymatic reactions with NTPs in the presence of a catalytic PNP mutant of DDAN$^{263–533}$. Peak intensities of each compound were normalized across all samples in the *in vitro* assays. Representative of three replicates.

(C) Catalytic mutant of DDAN does not convert dATP. LC-MS analysis of enzymatic reactions with dNTPs in the presence of a catalytic PNP mutant of DDAN$^{263–533}$. Peak intensities of each compound were normalized across all samples in the *in vitro* assays. Representative of three replicates.

(D) The NLR-like protein (called here NLRN) from the fungus *Hyaloscypha variabilis* harbors an N-terminal PNP domain (residues 2–308). TPR, tetratricopeptide repeat.

(E) Growth curves of *E. coli* cells expressing the NLRN PNP domain from the Lac promoter in conditions repressing expression (1% glucose, black) or inducing expression (1 mM ITPG, blue). Curves show the mean of three replicates with the standard deviation shown as a shaded area.

(F) Xanthine oxidase assays measuring adenine release from adenine-containing nucleotides by the NLRN PNP domain, as monitored by absorbance at 500 nm.